2. Carbon Cycle Greenhouse Gases

T.J. Conway (Editor), A.E. Andrews, L. Bruhwiler, A. Crotwell, E.J. Dlugokencky, M.P. Hahn, A.I. Hirsch
D.R. Kitzis, P.M. Lang, K.A. Masarie, A.M. Michalak, J.B. Miller, P.C. Novelli,
W. Peters, P.P. Tans, K.W. Thoning, B.H. Vaughn[1], and C. Zhao

2.1. Carbon Dioxide

2.1.1. In situ CO_2

The mixing ratio of atmospheric CO_2 was measured with continuously operating non-dispersive infrared analyzers (NDIR) at the four CMDL observatories during 2002 and 2003 as in previous years. Monthly and annual mean CO_2 concentrations, in the World Meteorological Organization 1985 Mole Fraction Scale (X85), are given in Table 2.1. These values are provisional, pending final calibrations of reference gas standards. Preliminary selected hourly average CO_2 mixing ratios for 2002 and 2003 are plotted for the four observatories in Figure 2.1.

From 5-15 May 2002, the CO_2 in situ sampling system was upgraded at the American Samoa Observatory (SMO). The measurement system was converted from two to three working standards. The system upgrade included a new computer and software and a new sample gas flow control system. The
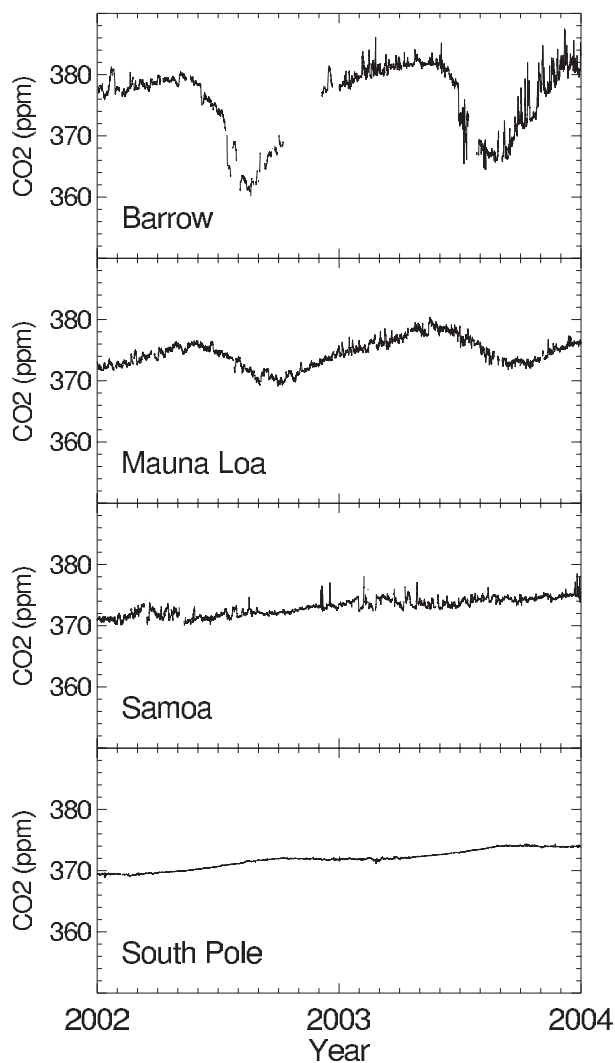
Table 2.1. Provisional 2002 and 2003 Monthly and Annual Mean CO_2 Mole Fractions from Continuous Analyzer Data (μmol mol^{-1}, Relative to Dry Air), for the Four CMDL Observatories

Month	BRW	MLO	SMO	SPO
2002				
Jan.	378.00	372.36	370.98	369.43
Feb.	377.67	373.09	371.49	369.33
March	378.33	373.81	372.47	369.52
April	379.16	374.93	371.99	369.76
May	379.21	375.58	371.12	370.02
June	376.15	375.44	371.28	370.42
July	369.94	373.86	371.97	370.92
Aug.	362.45	371.77	372.11	371.44
Sept.	366.36	370.73	372.01	371.80
Oct.	368.80	370.50	372.28	371.99
Nov.		372.18	372.96	371.95
Dec.	378.52	373.70	373.15	371.83
Year	374.05	373.16	371.98	370.70
2003				
Jan.	378.86	374.92	373.79	371.91
Feb.	380.84	375.62	373.69	371.83
March	381.14	376.51	374.38	371.97
April	381.85	377.75	373.85	372.12
May	381.86	378.54	373.49	372.45
June	380.06	378.20	373.34	372.78
July	371.57	376.68	374.09	373.21
Aug.	367.40	374.43	374.47	373.74
Sept.	369.34	373.11	374.25	374.03
Oct.	374.31	373.08	374.36	374.04
Nov.	379.20	374.76	374.70	373.93
Dec.	381.90	375.92	375.00	373.93
Year	377.36	375.79	374.12	373.00

μmol mol^{-1} is abbreviated as ppm.

Figure 2.1. Preliminary selected hourly mean CO_2 mole fractions in dry air expressed in μmol mol^{-1} at four CMDL observatories for 2002 and 2003.

---

[1]Institute for Arctic and Alpine Research, University of Colorado

base of the tower that holds the CO_2 intake sample lines was also replaced with a stainless steel version because the base integrity was compromised by rust. The fiberglass tower was lowered and all Dekoron intake lines from the tower top to the water separators in the pump house were replaced. The tower was then raised into the new tower base.

The CO_2 in situ analyzer at the Barrow, Alaska, Observatory (BRW) became increasingly noisy and unstable during fall of 2002. The Siemens Ultramat 5F analyzer was replaced on 5 December 2002 with a Licor Model 6251 CO_2 analyzer.

A new data acquisition system was installed at BRW in July 2003. This system uses a Linux workstation with an Intel CPU for controlling the CO_2 NDIR measurements. This system replaced the previous UNIX-based workstation. All four baseline observatories are now using the same type of computer, operating system, and control software. The data acquisition computer at the Mauna Loa, Hawaii, Observatory (MLO) was upgraded, and newer versions of the software were installed in November of 2003. The new software enables scientists in Boulder to view the same information on their workstation (virtual console) in Boulder that the operators see at MLO.

2.1.2. FLASK SAMPLE CARBON DIOXIDE MEASUREMENTS

A modest expansion of the CMDL Carbon Cycle Greenhouse Gases group (CCGG) Cooperative Global Air Sampling Network (Figure 2.2) began in 2002. The sampling network currently consists of 53 fixed locations, an increase of six sites since the previous Summary Report [*King et al.*, 2002]. The six new sampling locations are: Trinidad Head, California (THD), the CMDL west-coast observatory; Ochsenkopf, Germany, (OXK) a cooperative project with Max Planck Institute of Biogeochemistry (MPI-BGC), Jena, Germany; Pallas, Finland, (PAL) a GAW station; the Southern Great Plains ARM site, Oklahoma (SGP), a cooperative project with Lawrence Berkeley Laboratory; Mt. Kenya, Kenya, (MKN) a Global Atmosphere Watch (GAW) station; and the new tall tower site near Argyle, Maine, (AMT).

After a 2-year interruption, sampling across the Pacific Ocean resumed in 2002 aboard two container ships making regular voyages between Long Beach, California, and Auckland, New Zealand. The two new shipboard programs are aboard the *Columbus Waikato* and the *Kapitan Afanasyev*. Examples of the shipboard data are shown in Figures 2.3 and 2.4.
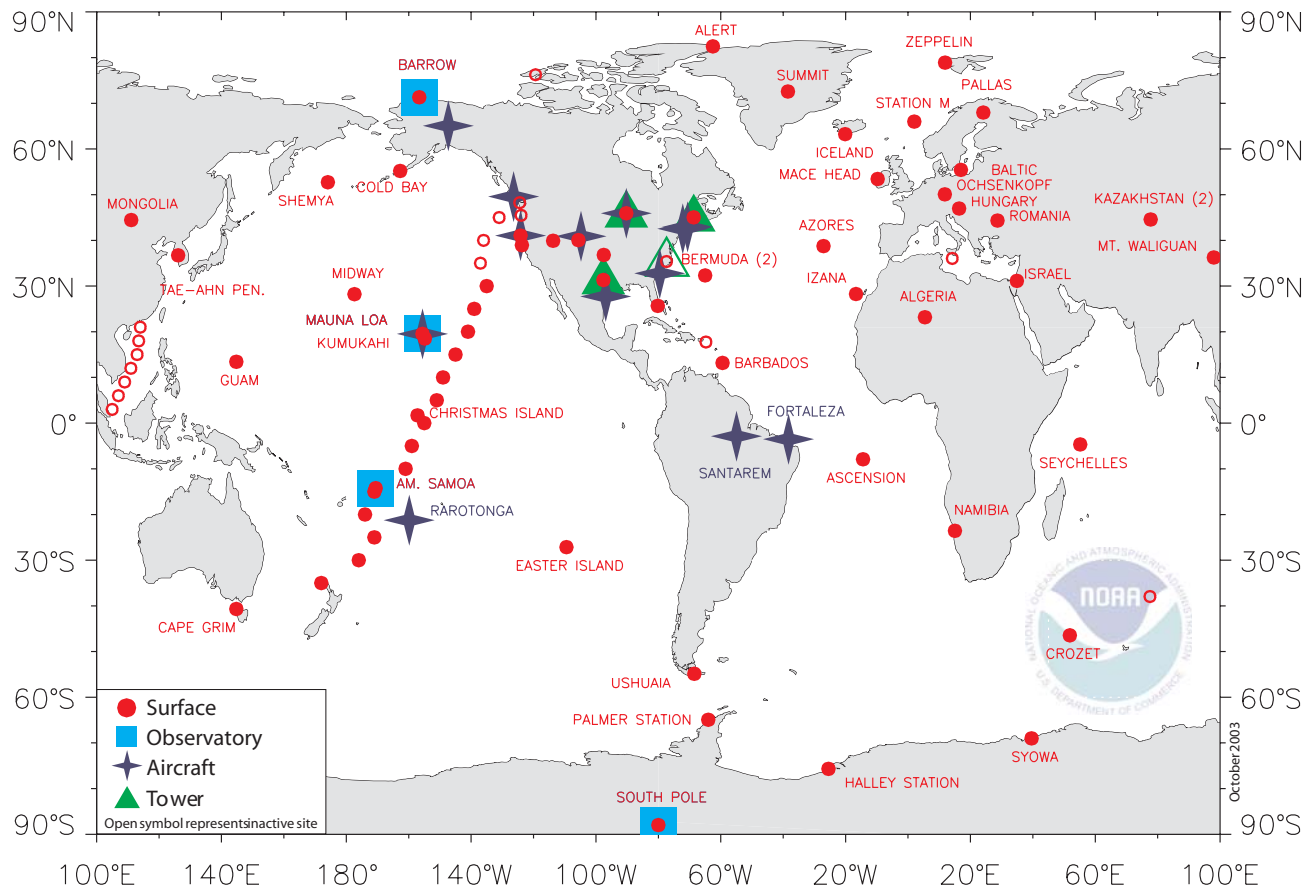

Figure 2.2. Locations of CCGG measurement programs, including baseline observatories (squares), Global Cooperative Air Sampling Network (circles), aircraft vertical profiles (stars), and the very tall tower sites (triangles).
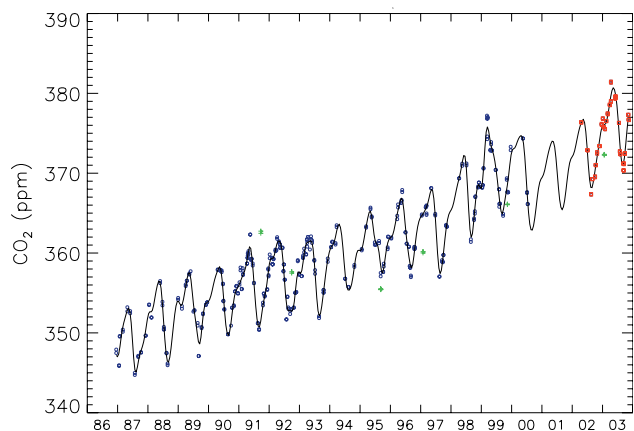
Figure 2.3. CO_2 mixing ratios measured in air samples collected aboard ships in the Pacific Ocean for the 5º latitude bin centered on 25º north latitude. Blue circles and red squares represent samples characteristic of the remote marine boundary layer. The green plus symbols represent flagged samples that are more than 3σ from the fitted smooth curve. The red squares represent samples collected on the *Columbus Waikato* and the *Kapitan Afanasyev* since the shipboard program resumed in 2002.
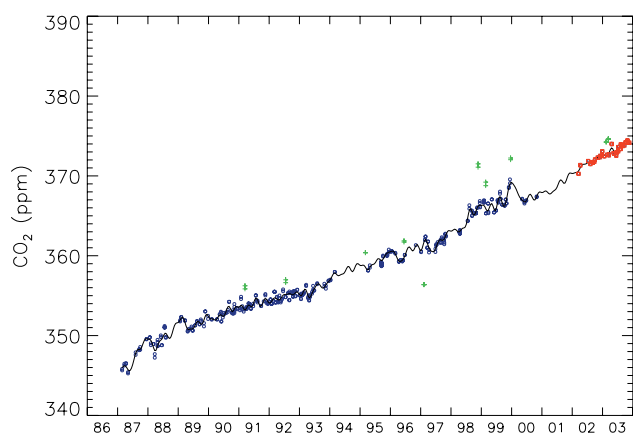

Figure 2.4. As in Figure 2.3, for 20º south latitude.

Throughout the network samples are collected approximately weekly (or at 5º latitude intervals on the ships) and returned to CMDL for analysis of CO_2, CH_4, CO, H_2, N_2O, and SF_6. The samples are then transported to the Stable Isotope Laboratory at the University of Colorado, Institute for Arctic and Alpine Research (INSTAAR) for analysis of $\delta^{13}C$ and $\delta^{18}O$ of CO_2. In 2002, 7200 samples were analyzed and 8300 were measured in 2003. Also, samples from 13 sites were measured at INSTAAR for $\delta^{13}C$ of CH_4.

The trace gas mixing ratios and isotopic measurements are available to the public and the scientific community from the CMDL Web site and FTP anonymous server. The measurements are used by modeling groups within and outside of CMDL to constrain estimates of CO_2 sources and sinks on global and semi-hemispheric scales. The measurements from the Global Network provide an important context for the intensive carbon measurement programs taking place in Europe and North America. A smoothed representation of the variation of atmospheric CO_2 with latitude and time, based on the network data, is given in Figure 2.5.

The 2002 and 2003 provisional annual mean mixing ratios for the six trace gases and the $\delta^{13}C$ values for CO_2 are given for 48 sites in Table 2.2. The $\delta^{13}C$ values for CH_4 are given for 11 sites in Table 2.2. Annual means for the shipboard samples for 2003 are given in Table 2.3. The global mean CO_2 mixing ratio and trend are plotted in Figure 2.6a from 1979 through 2003. The global CO_2 growth rate as a function of time (the derivative of the trend curve in Figure 2.6a) is plotted in Figure 2.6b. For 1979-2003 the globally averaged CO_2 growth rate is 1.6 ppm yr^{-1}. The growth rate in both 2002 and 2003 was higher than the average. From 2001 to 2002 the globally averaged CO_2 mixing ratio in the remote marine boundary layer increased by 2.0 ppm. From 2002 to 2003 CO_2 increased from 372.4 to 374.9, an increase of 2.5 ppm.

Two significant technical improvements were made in 2002-2003. A major redesign of the portable air sampler (AIRKIT) began in 2002 and the construction of the sampler was contracted to an outside vendor in 2003. The design improvements make the AIRKIT more rugged, more reliable, and easier to use in the field. Refinements to the design are continuing. A new 20-port flask preparation vacuum manifold was designed and constructed in 2003. This manifold will be used to test flasks for leaks and fill them with a conditioning gas before they are sent out to the sampling sites. The manifold is also used to fill the test flasks that are analyzed every day to monitor the performance of the analytical apparatus. The new manifold makes it easier to identify leaking flasks and is more efficient for flask preparation.
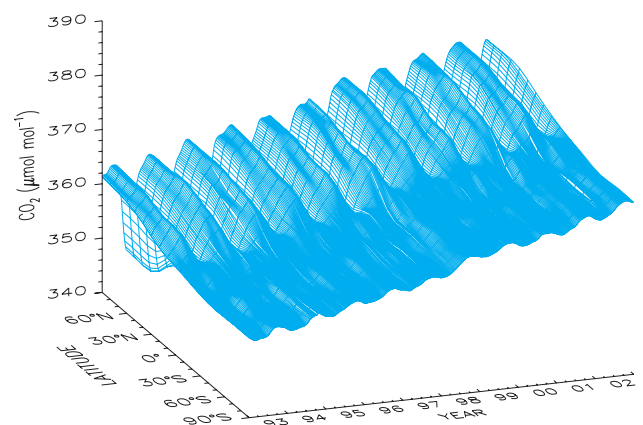

Figure 2.5. Data from the NOAA CMDL Cooperative Air Sampling Network show the three-dimensional representation of the latitudinal distribution of atmospheric carbon dioxide in the marine boundary layer. The surface represents data smoothed in time and latitude.

34

Table 2.2. Preliminary 2002 and 2003 Annual Mean Mixing and Isotopic Ratios From the CMDL CCGG
Cooperative Global Air Sampling Network

Site Code	Location	CO$_2$ (μmol mol^{-1}) 2002	2003	CH$_4$ (nmol mol^{-1}) 2002	2003	CO (nmol mol^{-1}) 2002	2003	N$_2$O (nmol mol^{-1}) 2002	2003	SF$_6$ (pmol mol^{-1}) 2002	2003	δ^{13}CO$_2$ (‰) 2002	2003	δ^{13}CH$_4$ (‰) 2002	2003
ALT	Alert, Nunavut, Canada	373.9	377.0	1830.2	1841.5	136.1	145.9	317.4	318.2	5.12	5.37	-8.20	-8.30	-47.36	-47.37
ASC	Ascension Island	371.8	374.2	1718.1	1718.6	72.7	72.4	317.0	317.7	4.88	5.11	-8.02	-8.06	-47.00	-46.97
ASK	Assekrem, Algeria	373.4	375.9	1778.9	1783.5	105.4	107.6	317.8	318.4	5.06	5.29	-8.10	-8.16	[ ]	[ ]
AZR	Terceira Island, Azores	373.7	375.7	1800.4	1814.6	109.6	131.7	317.1	317.5	5.11	5.35	-8.17	-8.24	[ ]	[ ]
BAL	Baltic Sea	378.8	384.1	[ ]	1880.6	178.2	193.0	318.2	319.4	5.44	5.56	-8.40	-8.66	[ ]	[ ]
BME	Bermuda (east coast)	373.9	376.6	1799.2	1818.7	125.5	134.2	317.6	318.5	5.13	5.41	-8.18	-8.20	[ ]	[ ]
BMW	Bermuda (west coast)	372.9	377.1	1790.5	1807.6	114.1	127.8	317.6	318.4	5.10	5.37	-8.09	-8.26	[ ]	[ ]
BRW	Barrow, Alaska	374.5	377.5	1839.3	1852.6	137.2	149.2	317.3	318.0	5.11	5.35	-8.25	-8.31	-47.43	-47.45
BSC	Black Sea, Romania	380.0	384.2	1910.8	1916.5	230.5	215.1	318.6	319.4	5.17	5.39	-8.48	-8.61	[ ]	[ ]
CBA	Cold Bay, Alaska	373.9	377.0	1827.4	1839.0	137.5	150.2	317.4	318.2	5.13	5.37	-8.22	-8.28	[ ]	[ ]
CGO	Cape Grim, Tasmania	370.7	372.9	1707.7	1709.0	52.8	52.6	316.1	316.8	4.82	5.05	-8.02	-8.06	-46.99	-46.93
CHR	Christmas Island, Kiribati	373.4	375.5	1728.9	1729.3	70.8	69.3	317.7	318.4	4.92	5.15	-8.04	-8.08	[ ]	[ ]
CRZ	Crozet Island	[ ]	[ ]	1708.2	1708.4	53.1	57.2	315.7	316.3	4.62	4.84	-8.02	-8.12	[ ]	[ ]
EIC	Easter Island	370.4	[ ]	1708.4	[ ]	63.6	[ ]	316.5	[ ]	4.84	[ ]	-8.02	[ ]	[ ]	[ ]
GMI	Mariana Islands, Guam	373.2	376.1	1765.6	1766.2	96.7	94.5	317.7	318.3	5.03	5.26	-8.09	-8.15	[ ]	[ ]
HBA	Halley Bay, Antarctica	370.6	[ ]	1706.6	[ ]	48.7	50.9	316.0	[ ]	4.84	[ ]	-8.04	[ ]	[ ]	[ ]
HUN	Hegyhatsal, Hungary	376.6	380.4	1891.4	1888.6	214.1	225.4	319.0	319.4	5.27	5.54	-8.44	-8.39	[ ]	[ ]
ICE	Heimaey, Iceland	373.8	376.7	1824.6	1835.4	135.1	140.9	317.7	318.4	5.12	5.39	-8.18	-8.28	[ ]	[ ]
IZO	Izaña Obs., Tenerife	372.8	[ ]	1784.4	1788.6	101.4	106.2	317.8	318.4	5.09	5.31	-8.06	-8.12	[ ]	[ ]
KEY	Key Biscayne, Florida	374.3	377.7	1786.3	1806.7	110.3	124.2	317.7	318.3	5.10	5.35	-8.12	-8.23	[ ]	[ ]
KUM	Cape Kumukahi, Hawaii	373.5	376.4	1777.3	1786.8	106.5	123.9	317.6	318.2	5.06	5.30	-8.11	-8.23	-47.11	-47.09
KZD	Sary Taukum, Kazakhstan	377.9	380.4	1839.0	1853.3	150.7	147.1	317.9	318.6	5.12	5.36	-8.40	-8.50	[ ]	[ ]
KZM	Plateau Assy, Kazakhstan	373.1	377.3	1816.6	1826.9	139.5	146.7	317.8	318.5	5.10	5.35	-8.11	-8.35	[ ]	[ ]
LEF	Park Falls, Wisconsin	376.4	381.9	1856.3	1878.3	154.1	159.0	317.9	318.3	5.15	5.38	-8.11	-8.35	[ ]	[ ]
MHD	Mace Head, Ireland	373.5	376.4	1822.4	1827.9	138.9	142.6	317.5	318.4	5.14	5.38	-8.25	-8.24	[ ]	[ ]
MID	Sand Island, Midway	373.3	376.2	1790.6	1804.4	116.3	130.6	317.6	318.4	5.10	5.35	-8.12	-8.18	[ ]	[ ]
MLO	Mauna Loa, Hawaii	373.0	375.8	1761.6	1770.2	96.2	100.2	317.6	318.3	5.01	5.26	-8.09	-8.16	-47.13	-47.10
NWR	Niwot Ridge, Colorado	374.2	376.4	1801.8	1803.4	130.6	129.9	317.9	318.6	5.10	5.33	-8.18	-8.18	-47.16	-47.11
PAL	Pallas, Finland	374.6	376.3	[ ]	[ ]	134.3	129.7	[ ]	[ ]	[ ]	[ ]	[ ]	[ ]	[ ]	[ ]
PSA	Palmer Station, Antarctica	370.8	[ ]	1708.1	[ ]	63.6	[ ]	316.3	[ ]	4.81	[ ]	-8.04	-8.08	[ ]	[ ]
PTA	Point Arena, California	377.0	[ ]	1813.12	[ ]	122.7	145.4	318.5	[ ]	5.13	[ ]	-8.23	[ ]	[ ]	[ ]
RPB	Ragged Point, Barbados	373.0	375.6	1771.10	1773.1	79.3	82.2	317.6	318.4	5.04	5.27	-8.08	-8.14	[ ]	[ ]
SEY	Mahé Island, Seychelles	372.4	[ ]	1728.3	[ ]	79.2	79.6	317.4	[ ]	4.91	5.12	-8.03	-8.07	[ ]	[ ]
SGP	So. Great Plains, Oklahoma	[ ]	378.3	[ ]	1886.6	[ ]	111.4	[ ]	318.9	[ ]	5.43	[ ]	-8.30	[ ]	[ ]
SHM	Shemya Island, Alaska	374.2	377.1	1826.3	1835.6	139.8	133.6	317.6	318.4	5.13	5.37	-8.17	-8.30	[ ]	[ ]
SMO	American Samoa	371.9	374.1	1711.3	1713.0	66.9	61.2	316.8	317.4	4.87	5.10	-8.01	-8.05	-47.01	-47.98
SPO	South Pole, Antarctica	370.6	372.9	1708.4	1708.8	63.8	63.8	315.9	316.7	4.82	5.04	-8.03	-8.08	-46.97	-46.95
STM	Ocean Station M	373.3	376.8	1828.1	1838.0	130.5	128.9	317.6	318.3	5.12	5.38	-8.21	-8.31	[ ]	[ ]
SUM	Summit, Greenland	[ ]	[ ]	[ ]	[ ]	[ ]	[ ]	[ ]	[ ]	[ ]	[ ]	[ ]	[ ]	[ ]	[ ]
SYO	Syowa Station, Antarctica	370.8	[ ]	1708.1	[ ]	63.1	[ ]	315.9	[ ]	[ ]	[ ]	-8.04	[ ]	[ ]	[ ]
TAP	Tae-ahn Pen., Rep. of Korea	377.8	379.6	1865.8	1871.6	272.9	223.9	318.4	319.1	5.18	5.42	-8.38	-8.45	-47.36	-47.37
TDF	Tierra del Fuego, Argentina	370.8	[ ]	[ ]	[ ]	[ ]	[ ]	[ ]	[ ]	[ ]	[ ]	-8.05	[ ]	[ ]	[ ]
UTA	Wendover, Utah	374.7	377.3	1806.5	1810.8	135.0	133.4	317.8	318.6	5.11	5.38	-8.20	-8.24	[ ]	[ ]
UUM	Ulaan Uul, Mongolia	374.3	377.8	1828.1	1836.6	170.6	175.5	317.7	318.4	5.13	5.37	-8.22	-8.30	[ ]	[ ]
WIS	Negev Desert, Israel	375.2	377.9	1832.4	1843.6	150.9	159.1	318.2	318.9	5.17	5.38	-8.21	-8.31	[ ]	[ ]
WKT	Moody, Texas	376.6	378.9	1845.4	1858.8	[ ]	[ ]	317.9	318.8	5.27	5.43	-8.27	-8.27	[ ]	[ ]
WLG	Mt. Waliguan, P.R. of China	372.6	376.0	1798.8	1812.6	144.7	140.9	317.7	318.4	5.09	5.37	-8.11	-8.25	-47.21	-47.19
ZEP	Ny-Ålesund, Svalbard	374.4	377.0	1832.9	1843.4	140.1	147.5	317.6	318.3	5.13	5.37	-8.24	-8.27	[ ]	[ ]

Note: Square brackets indicate insufficient data to calculate the annual mean.

Table 2.3. Preliminary 2003 Annual Mean Mixing and Isotopic Ratios from the CMDL CCGG Pacific Ocean Shipboard Air Samples

Latitude	CO_2 (μmol mol^{-1}) 2003	CH_4 (nmol mol^{-1}) 2003	CO (nmol mol^{-1}) 2003	N_2O (nmol mol^{-1}) 2003	SF_6 (pmol mol^{-1}) 2003	$\delta^{13}CO_2$ (‰) 2003
30°N	375.9	1805.4	128.0	318.3	5.32	-8.21
25°N	376.4	1797.0	120.9	318.2	5.34	-8.19
20°N	376.4	1789.5	112.6	318.3	5.32	-8.21
15°N	376.3	1778.2	102.2	318.4	5.29	-8.16
10°N	375.9	1760.1	90.9	318.4	5.24	-8.12
5°N	375.7	1740.5	75.9	318.5	5.18	-8.08
Equator	375.5	1727.9	67.6	318.3	5.13	-8.07
5°S	375.2	1723.3	61.1	318.1	5.15	-8.06
10°S	374.6	1718.2	60.3	317.9	5.11	-8.06
15°S	374.3	1712.8	57.8	317.7	5.11	-8.05
20°S	373.4	1712.1	57.1	317.2	5.08	-8.06
25°S	373.2	1710.9	55.7	317.1	5.07	-8.05
30°S	373.1	1710.1	54.1	317.0	5.06	-8.06
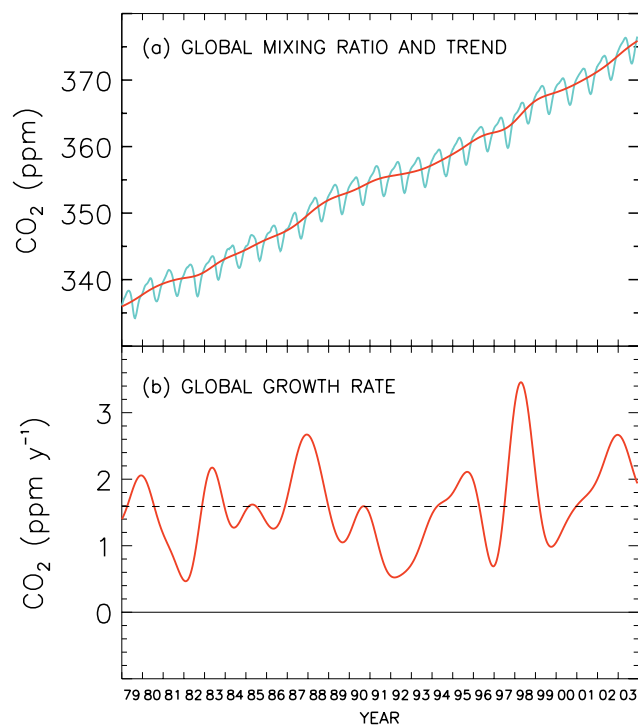
Figure 2.6. (a) The globally averaged CO_2 mixing ratio versus time for 1979-2003 (blue curve) based on samples collected at remote marine boundary layer sites of the CCGG Cooperative Global Air Sampling Network. The red curve in (a) represents the long-term global trend with the seasonal variation filtered out. The red curve in (b) is the first derivative with respect to time of the trend curve (red) in (a) and represents the variation of the global CO_2 growth rate versus time.

Since 1992 air samples have been collected aboard a ferry boat making regular crossings of the Baltic Sea. Our Polish colleague in this project, and the captain and mates of the *Stena Baltica* were awarded the NOAA Environmental Hero Award in June 2003. This award was in recognition of their ongoing and conscientious efforts to assist NOAA and CMDL in achieving their missions. The awards were presented by the U.S. Ambassador to Poland during a ceremony at the United States Embassy in Warsaw.

2.1.3. THE CARBON DIOXIDE CALIBRATION SCALE AND REFERENCE GAS CALIBRATIONS

The 15 WMO primary standards, ranging in CO_2 mole fraction from approximately 250 to 520 μmol mol^{-1}, were calibrated at regular intervals (between 1 and 2 years) by CMDL's manometric system [*Zhao et al.*, 1997]. The function of the primary standards is to provide continuity to the WMO scale, as well as a quality-control check on the performance of the manometric system. The fifth set of manometric calibrations of the 15 WMO primary standards was completed in April 2003. From September 1996 through August 2003 there are a total of 301 individual manometric determinations in these analyses. The results are summarized in Table 2.4. The mean precision of the manometric measurements indicated in Table 2.4 as the standard deviations is about 0.08 μmol mol^{-1}. For comparison, the CO_2 mole fractions measured by the Scripps Institution of Oceanography (SIO) using the infrared absorption technique are also shown in Table 2.4. The CO_2 values shown in Table 2.4 are the mean of each group of calibrations for both CMDL and SIO. The SIO CO_2 analysis data in Table 2.4 are the revisions (called the X99A scale by SIO) received by CMDL in early 2002. When the WMO CO_2 Experts Meeting transferred responsibility for maintaining the WMO Scale from SIO to CMDL in 1995, the values assigned to the 15 WMO primaries were still based entirely on the calibrations by Scripps. From mid-1996 to early 2001, the assigned CO_2 values of the 15 primaries were jointly based on the SIO and CMDL measurements, and from 2001 to the present, completely based on the CMDL measurements alone. For the primary standards in the atmospheric CO_2 concentration range of 300 to 400 μmol mol^{-1} the concentrations analyzed by our manometric method are on average about 0.05 μmol mol^{-1} higher than the SIO NDIR analyses relative to the WMO X93 scale. After the X99A revisions by SIO, the difference with CMDL became much smaller and is only 0.02 ppm lower than CMDL in the ambient range of 345-420 ppm.

Table 2.4. Summary of Measurements of the WMO Primary CO_2 Standards Expressed as $\mu mol\ mol^{-1}$ in Dry Air (ppm), September 1996-April 2003

Cylinder Serial Number	N	CMDL		SIO		Difference (mano−old)*
		(ppm)	(1σ)	(ppm)	(1σ)	(ppm)
110	20	246.67	0.10	246.59	0.08	0.08
102	23	304.37	0.06	304.35	0.09	0.02
111	18	324.01	0.09	324.01	0.05	0.00
130	17	337.26	0.06	337.27	0.02	0.01
121	21	349.39	0.05	349.36	0.01	0.03
103	19	353.31	0.10	353.20	0.03	0.11
139	20	360.90	0.02	360.87	0.06	0.03
105	18	369.37	0.03	369.40	0.06	-0.03
136	20	381.33	0.08	381.34	0.08	0.01
146	21	389.54	0.04	389.60	0.08	-0.06
101	18	396.33	0.12	396.30	0.07	0.03
106	21	412.08	0.10	412.08	0.12	0.00
123	24	423.07	0.12	423.05	0.13	0.02
107	26	453.10	0.12	452.96	0.16	0.14
132	20	521.41	0.16	521.07	0.64	0.34

*Difference between CMDL manometric values and values determined with the SIO X99A scale.

To maximize the useful life span of the primaries, the calibration scale is transferred via NDIR measurements approximately twice a year to a set of secondary standards. These in turn are used to calibrate, via NDIR comparisons, every other cylinder. During 2002 about 700 cylinders were calibrated with this method to give each a WMO mole fraction value for CO_2. The precision, or repeatability, in the range between 250 and 520 $\mu mol\ mol^{-1}$, has been generally about 0.01 $\mu mol\ mol^{-1}$.

On request, calibrations are performed with the manometric system well outside of the range of atmospheric CO_2 values. Because there was some demand for calibrations well above 520 $\mu mol\ mol^{-1}$, new primary CO_2 standards were created at the high end of the range at approximately 600, 700, 1000, 1500, 2000, 2500, and 3000 $\mu mol\ mol^{-1}$. These standards allow efficient CO_2 calibrations using the comparative infrared absorption technique.

Cylinders prepared by CMDL with a specified CO_2 concentration undergo the following procedures at the clean-air pumping station at high elevation on Niwot Ridge (NWR), east of Boulder [*Kitzis et al.,* 1999]. For a new or recently hydrotested cylinder: (1) The cylinder is vented and then pressurized twice with dry natural air to about 20 atm (300 psi) and vented again. (2) The cylinder is filled to about 34 atm (510 psi) with dry natural air and stored for several weeks. (3) Before the final fill the cylinder is first vented and then spiked with a small amount of either 10% or zero CO_2-in-air, depending on the desired final mixing ratio. (4) The cylinder has a final fill with compressed and dried ambient natural air to 135 atm (2000 psi), during which the ambient CO_2 mixing ratio is monitored. (5) The water vapor content of the filled cylinder is measured; it must be less than 5 ppm and is usually about 1 ppm. Drying is accomplished using a magnesium perchlorate ($Mg\ (ClO_4)_2$) trap. The pump is a RIX oil-less diving compressor. For a previously used cylinder: Steps 1 and 2 are replaced by venting and one fill with dry natural air to a pressure of 20 atm. Other trace gases, such as CH_4 and CO, can be targeted to specified values in the same cylinders.

2.1.4. ISOTOPES OF GREENHOUSE GASES

The Stable Isotope Laboratory at INSTAAR works closely with CMDL's Carbon Cycle Greenhouse Gases Group (CCGG) to measure stable isotope ratios of atmospheric greenhouse gases. We currently measure $\delta^{13}C$ and $\delta^{18}O$ of atmospheric CO_2 in nearly all of the CMDL CCGG Cooperative Global Air Sampling Network samples, samples from tall towers, and aircraft samples. Currently there are 53 active stationary sites, multiple ship sampling tracks, and 13 aircraft sampling sites using Programmable Flask Packages (PFPs). A total of 13,198 isotopic measurements were made in 2003 on atmospheric CO_2 in flasks, reference cylinders, and PFPs combined (Table 2.5). A set of 13 sites is also measured for $\delta^{13}C$ of atmospheric CH_4. A system to measure δD in atmospheric CH_4 is also in test phase, as well as a method for isotopes in water vapor extracted from the NOAA flasks. Planned future analyses include isotopes of atmospheric CO, N_2O, and H_2.

$\delta^{13}C$ of Atmospheric CO_2

A current plot of $\delta^{13}C$ of CO_2 variation with time and latitude is shown in Figure 2.7. This data is essential to separating fluxes of atmospheric CO_2 between the terrestrial biosphere and the ocean [*Tans et al.,* 1993]. Plants discriminate against $^{13}CO_2$ during photosynthesis by about −18‰ [*Lloyd and Farquhar*, 1994]. This is a very large effect compared to the few per mil fractionation that occurs when CO_2 goes into and out of the surface ocean [*Zhang et al.*, 1995]. Figure 2.8 shows carbon fluxes divided into oceanic and terrestrial components derived using a two-dimensional model of atmospheric transport [*Ciais et al.*, 1995].

$\delta^{18}O$ of Atmospheric CO_2

Measurements of $\delta^{18}O$ of CO_2 are ongoing at all network sites. Significant efforts were made to identify high humidity sites in the flask network and to ensure that air samples obtained from these sites are dried in situ to minimize the oxygen exchange

Table 2.5. Isotopic Measurements Made at the Stable Isotope Laboratory, INSTAAR, University of Colorado*

Year	Total Samples	Flasks	Aircraft PFP's	Calibration Tanks	Reference Tanks
1990	3598	2570	0	0	1028
1991	6444	4603	0	0	1841
1992	8981	6415	0	0	2566
1993	7325	5232	0	0	2093
1994	9447	6562	102	84	2699
1995	10,534	6875	185	464	3010
1996	10,860	7407	118	232	3103
1997	11,385	7597	99	436	3253
1998	10,527	7118	101	300	3008
1999	11,413	7153	139	860	3261
2000	12,053	6375	898	1336	3444
2001	9478	5254	904	612	2708
2002	11,165	5917	1006	1052	3190
2003	13,198	6765	1814	848	3771

*Values are listed for the number of measurements of $d^{13}C$ and $d^{18}O$ of CO_2 made on CMDL network flasks, Programmable Flask Packages (PFPs), as well as reference tanks and calibration tanks.
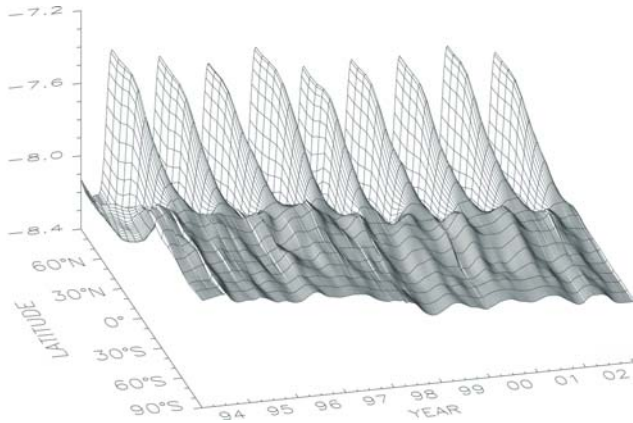
Figure 2.7. Three-dimensional representation of the latitudinal distribution of the carbon isotopic composition of atmospheric carbon dioxide in the marine boundary layer. The measurements of stable isotope ratios were made at INSTAAR (University of Colorado) using air samples provided by the CMDL Cooperative Global Air Sampling Network. The surface represents data smoothed in time and latitude. The isotope data are expressed as deviations of the $^{13}C/^{12}C$ ratio in carbon dioxide from the VPDB-CO_2 standard in per mil (parts per thousand, or ‰).

between the water and the CO_2 in the flask during storage and transit [*Gemery et al.*, 1996]. It is unclear whether this process can explain similar issues with cold and dry sites such as South Pole (SPO). Historical CO_2 $\delta^{18}O$ data collected from problem sites, typically low latitude sites, is evaluated for inclusion in the global data set where it is determined to be meaningful. Many other sites are still producing excellent CO_2 $\delta^{18}O$ data, and seasonal trends are very prominent at high northern latitude sites such as Barrow, Alaska (Figure 2.9).

Programmable Flask Packages

PFPs have been used to acquire air samples from aircraft since 1994. The measurement of PFPs has increased by more than an order of magnitude since 1999 (Table 2.5) and is projected to continue to grow as PFPs are used at more sites. Currently all isotopic measurements on PFPs are performed on the same mass spectrometer used to measure the network flasks. The advantage is automatic calibration of PFPs to flasks and reference tanks because the measurements are all made on one instrument. The disadvantage is the instrument is operating at maximum capacity (24 hours a day, 7 days a week) to handle the current analysis load. To accommodate the anticipated increased analysis load, an additional mass spectrometer was purchased (funded in part through the NOAA Global Change Program), and the construction of a dedicated CO_2 extraction system is underway. The new system will handle up to four PFPs (12 flasks each) connected to the instrument along with the necessary calibration cylinders and use protocols for extraction and analyses identical to the flask analyses instrument. Intercalibration between the two instruments is essential and will be accomplished with reference
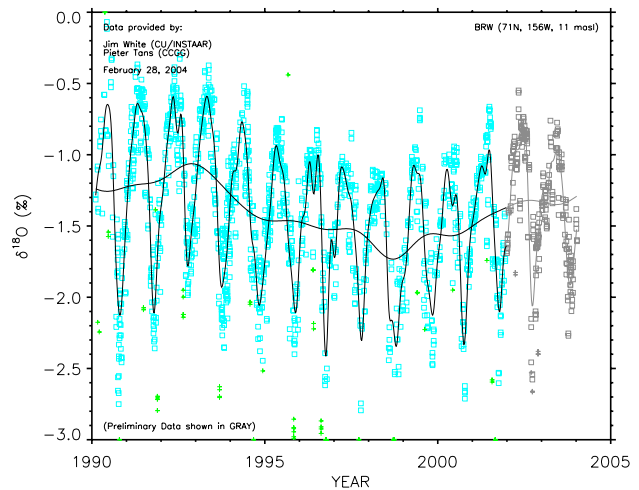

Figure 2.8. Surface fluxes of CO_2 (after correction for fossil fuel fluxes) in five latitude zones. Total fluxes in each zone (red curve) are divided into oceanic (blue) and terrestrial (green) fluxes. Negative numbers indicate a sink of carbon into either the ocean or land biosphere, and positive ones indicate a source.

Figure 2.9. Measurements of $\delta^{18}O$ of atmospheric CO_2 at Barrow, Alaska. Time series from air collected approximately weekly in glass containers and returned to CCGG for analysis. Squares are thought to be regionally representative; pluses are thought to be influenced by local sources and sinks. A smooth curve and long-term trend are fitted to the representative measurements when sufficient data exist. Data shown in gray are preliminary. All other data have undergone rigorous quality assurance and are freely available from CMDL.

tanks and PFP comparisons. In addition, this will provide an instrumental check on intercomparisons of standard gases between other laboratories.

Experience has shown that one dedicated mass spectrometer can handle approximately 10,000 analyses per year. We currently measure PFPs from 13 sites at a frequency of one flight per month, or about 1800 PFP sample flasks per year. Plans call for an increase in the frequency of flights to once per week at 7 of the 13 sites. Along with other planned additions to the PFP network, it is estimated that by the end of fiscal year 2004 we will be analyzing 76 PFPs (or 912 flasks) per month. By 2007 the NOAA plan is to add about 15 more North American Carbon Program (NACP) sites and at least 5 more international sites, bringing the analyses load to 180 PFPs (or 2,160 flasks) per month (Figure 2.10). Using the approximate capacity of 10,000 analyses per dedicated mass spectrometer, CCGG will need to increase its analytical capacity for PFPs by 2.4 times the level established in 2004.

$\delta^{13}C$ of Atmospheric CH_4

Using an automated system for the analysis of $\delta^{13}C$ in atmospheric methane in small volume air samples [*Miller et al.*, 2002], pairs of flasks are analyzed on a weekly basis from 13 sites of the CMDL CCGG Cooperative Global Air Sampling Network (Table 2.6). CCGG has now measured about 6000 individual flasks for $\delta^{13}C$ of CH_4. Time series of CH_4 and its $\delta^{13}C$ from BRW are shown in Figure 2.11 for reference. The analytical precision of the measurements is about 0.07‰, as determined by the repeatability of reference gas aliquots treated as unknowns and is comparable to the mean difference of flask pairs collected at network sites. Our standard scale is linked to a scale maintained by the University of California, Irvine (UCI). Our own suite of working reference tanks was established based on this scale, and comparisons of air sampled at NWR and measured separately at UCI and INSTAAR show good agreement.

Figure 2.12 shows global annual average fluxes derived from global annual average CH_4 and $\delta^{13}C$ measurements, using equations 1 and 2. For this analysis, only sites in operation since 1998 were used. All methane emissions, Q, and their isotopic ratios, δ, are divided into three categories, 'micr' (microbial), 'ff' (fossil fuel), and 'bmb' (biomass burning), which reflect sources having similar isotopic ratios.

$$Q = Q_{micr} + Q_{ff} + Q_{bmb} \qquad (1)$$

$$\delta_q Q = \delta_{micr}Q_{micr} + \delta_{ff}Q_{ff} + \delta_{bmb}Q_{bmb} \qquad (2)$$

Q is calculated using CH_4 data alone, according to equation (3), and δ_q is calculated using just isotopic information in equation (4).

$$\frac{d[CH_4]}{dt} = Q - \frac{[CH_4]}{\tau} \qquad (3)$$

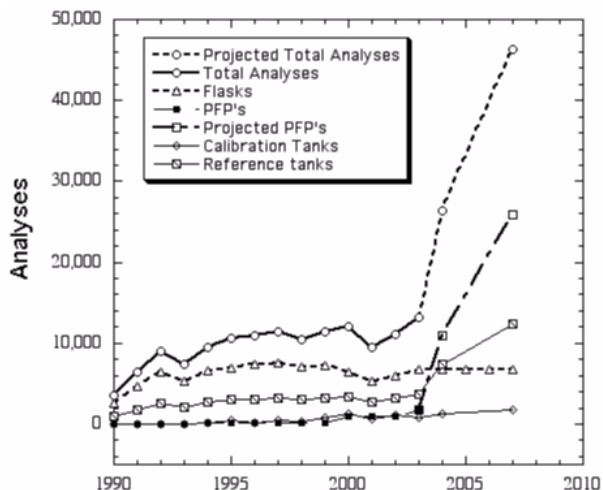$$\delta_q = \delta_a + \varepsilon \qquad (4)$$

Figure 2.10. Stable isotope analyses 1990 through 2003 and projected 2004-2007. Total analyses line represents the sum of all analyses types, including network flasks, PFPs, internal reference tanks, and periodically analyzed calibration tanks for our laboratory and others. Large projected analyses in 2004 through 2007 are due to expected increase in PFP analyses.

In equation 3, τ is the lifetime of CH_4 with respect to its destruction by OH [*Montzka et al.*, 2000] and other processes [*Hein et al.*, 1997]; in equation 4, ε is the average isotopic fractionation associated with these processes [*Cantrell et al.*, 1990]. From atmospheric measurements Q and δ_q are known, and from field studies values of δ_{micr}, δ_{ff}, and δ_{bmb} are assigned, but in order to solve equations 1 and 2 as a system of two equations with two unknowns, $^{14}CH_4$ data [*Quay et al.*, 1999] is used to specify Q_{ff}. Although there is uncertainty in the fossil fuel flux of about 50% and uncertainty in the values of τ and ε, the true values are unlikely to change much over this time period implying that the annual changes in the microbial and biomass burning fluxes are robust.

Table 2.6. Measured $\delta^{13}C$ of CH_4 Flask Sites

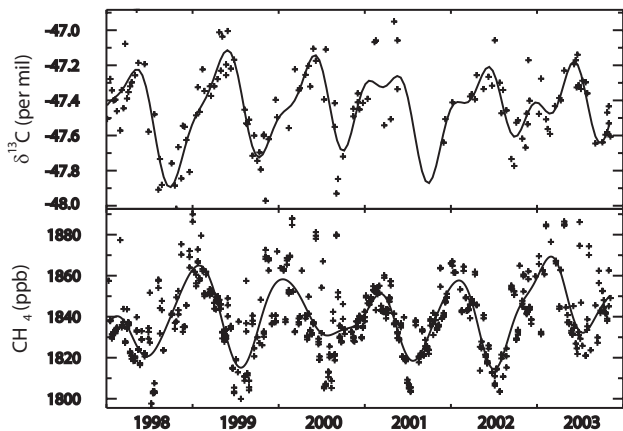| Site	Latitude	Longitude	Start Date
ALT	82.45°N	62.52°W	Jan. 2001
ASC	7.92°S	14.42°W	Jan. 2001
AZR	38.77°N	27.38°W	Jan. 2001
BRW	71.32°N	156.6°W	Jan. 1998
CGO	40.68°S	144.68°E	Jan. 1998
KUM	19.52°N	154.82°W	Jan. 1999
MHD	53.33°N	9.9°W	Jan. 2001
MLO	19.53°N	155.58°W	Jan. 1998
NWR	40.05°N	105.58°W	Jan. 1998
SMO	14.25°S	170.57°W	Jan. 1998
SPO	89.98°S	24.8°W	Jan. 1998
TAP	36.73°N	126.13°E	Jan. 2001
WLG	36.29°N	100.9°E	Jan. 2001

Figure 2.11. Pair averages of δ^{13}C of CH_4 and the corresponding CH_4 values from the same flask pairs at Barrow, Alaska. The lines are smooth curves fitted to the data that help to identify the seasonal cycle. For δ^{13}C of CH_4, some data is missing in 2001 due to analysis problems.
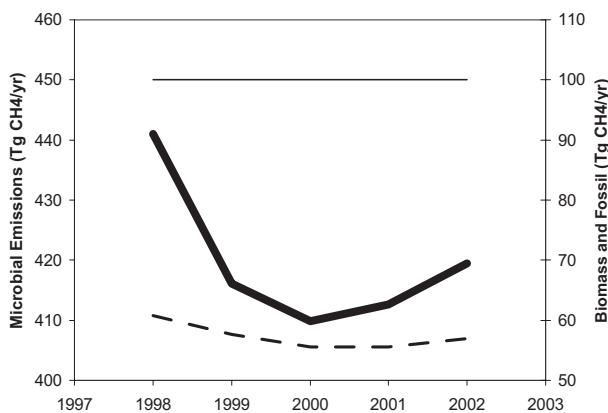

Figure 2.12. Global microbial (thick solid line, left-hand axis) and biomass burning (thick dashed line, right-hand axis) fluxes derived from global, annual average CH_4 and δ^{13}C data between 1998 and 2002 (see text for details). Here, fossil fuel fluxes (thin line, right-hand axis) are determined using $^{14}CH_4$ measurements [*Quay et al.*, 1999]. Note that the two axes have the same scale; therefore, the microbial and biomass burning fluxes are directly comparable.

The analysis shows that microbial emissions dominated the large methane anomaly observed in 1998, and biomass burning emissions contributed very little (about 20%). While this is consistent with the earlier analysis from the work of *Dlugokencky et al.* [2001], it strongly disagrees with a recent analysis of biomass burning in the work of *van der Werf et al.* [2004]. The *van der Werf et al.* [2004] study used a combination of satellite-based fire data, a fire model, and atmospheric data to infer that all of the global CH_4 growth rate anomaly could be attributed to fires. If the entire growth rate anomaly was due to fire, model simulations indicate that the global average atmospheric change in δ^{13}C of CH_4 between 1998 and 1999 would decline by 0.002‰ where, in fact, it was observed to increase by 0.05‰. Although

these signals are near our detection limit, they cast doubt on the *van der Werf et al.* [2004] hypothesis.

2.2. METHANE, NITROUS OXIDE AND SULFUR HEXAFLUORIDE

2.2.1. IN SITU METHANE MEASUREMENTS

Quasi-continuous measurements of atmospheric methane continued at MLO and BRW at a frequency of four ambient measurements each hour. The chromatographic scheme at MLO was changed during 5-6 November 2003. The two-column system that was plumbed into a 10-port sample/inject valve (pre- and analytical columns) was replaced by a single 3-m HayeSep Q column plumbed into a 6-port valve. Advantages of the new system are smaller rates of carrier gas consumption and better measurement repeatability. Relative precisions are currently ~0.07% at BRW and ~0.05% at MLO. Details of the measurement techniques and analysis of the in situ data through early 1994 were published in the work of *Dlugokencky et al.* [1995]. Daily averaged methane mole fractions (in nmol mol^{-1}) are plotted in Figure 2.13 for BRW (a) and MLO (b). The data were edited for instrument malfunction using a rule-based expert system [*Masarie et al.*, 1991], and they were selected for meteorological conditions. The BRW data are constrained to the clean air sector that includes wind directions of 020° to 110° and wind speeds ≥1 m s^{-1}. MLO data are constrained to 0000-0659
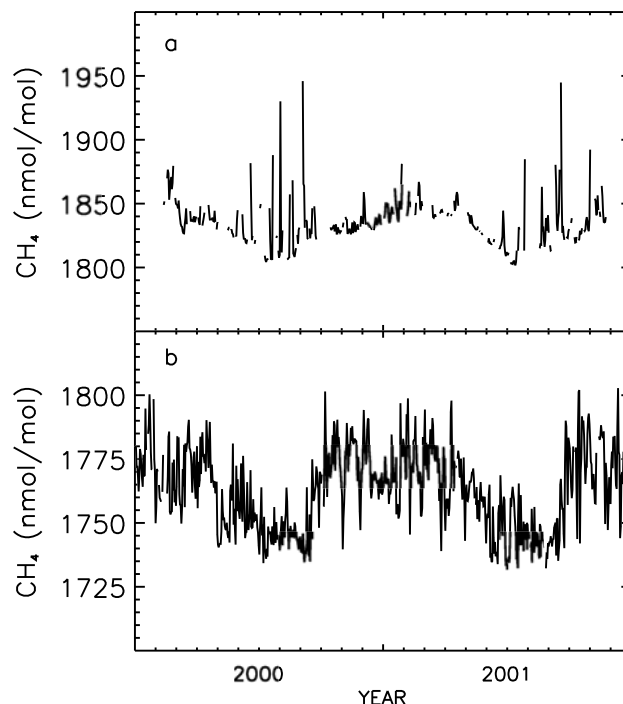

Figure 2.13. Daily mean CH_4 mole fractions in nmol mol^{-1} for (a) Barrow and (b) Mauna Loa for 2002 and 2003. The data are constrained for wind regime (see text) and they have undergone a quality control step to ensure that the analytical instrument was working optimally when they were obtained [*Masarie et al.,* 1991].

40

local time, which are typically periods with down-slope winds. In situ data are available at hourly, daily, and monthly time resolution from the CMDL World Wide Web page (www.cmdl.noaa.gov) or FTP file server's "pub" directory (ftp.cmdl.noaa.gov).

2.2.2. MEASUREMENTS OF METHANE IN DISCRETE SAMPLES

During 2002-2003 the determination of the global distribution of atmospheric methane continued from 47 sampling sites of the CMDL CCGG Cooperative Global Air Sampling Network. Sampling was started at six new sites during this 2-year period. North-to-south sampling transects of the Pacific Ocean on two ships began again during March 2002. Air sampling also began from a tower at Argyle, Maine, in September 2003; Ochsenkopf, Germany, in March 2003 as part of a flask-intercomparison experiment with Max Planck Institute for Biogeochemistry, Jena; Pallas-Sammaltunturi, Finland, in December, 2001; Oklahoma, at the SGP site in collaboration with Lawrence Berkeley National Laboratory in April 2002; Trinidad Head in April, 2002; and Mt. Kenya, Kenya, at the GAW Observatory. Complete data records and monthly means can be obtained through 2003 for each site from the CMDL world wide web page (www.cmdl.noaa.gov) or FTP file server's "pub" directory (ftp.cmdl.noaa.gov). A three-dimensional representation of the distribution of atmospheric CH_4 versus latitude and time is shown in Figure 2.14.

Globally averaged CH_4 dry-air mole fractions are plotted in Figure 2.15a for June 1983 through 2002 [see *Dlugokencky et al.,* 1994a for further details on calculation of global and zonal averages]. Atmospheric methane increased from about 1615 nmol mol^{-1} at the start of the record to about 1750 nmol mol^{-1} during 1999 and then remained nearly constant from 1999 through 2002 [*Dlugokencky et al.,* 2003]. The instantaneous growth rate for globally averaged CH_4 is plotted in Figure 2.15b; it has decreased from about 14 nmol mol^{-1} yr^{-1} at the start of the record to approximately no increase from 2000 to 2002 with significant interannual variability. An attempt has been made to explain the large variations in growth rate. The increased global growth rate in 1991 appears to be driven by CH_4 sink chemistry in the tropics after the eruption of Mt. Pinatubo in July, 1991. *Dlugokencky et al.* [1996] showed that SO_2 emitted during the eruption, and subsequent sulfate aerosol produced by oxidation of the SO_2, affected tropical photochemistry that temporarily increased the CH_4 growth rate. The decreased global growth rate during 1992 was driven by a decrease of 0.3 ±0.8 nmol mol^{-1} in the Northern Hemisphere. *Dlugokencky et al.* [1994b] suggested the decreased growth rate in 1992 could, only in part, be explained by decreased emissions from natural wetlands. A process-based model (B. Walter, personal communication, 2000) was used to show that lower-than-normal temperatures and precipitation in high northern wetland regions during 1992 resulted in decreased CH_4 emissions from wetlands. Such a change in wetland emissions would have been temporary; there is now evidence in the measurements that a separate, permanent step-like decrease in high northern emissions occurred during 1992 (see later in this section). During 1998 there was a large positive anomaly in global growth rate that corresponded to an increase in the imbalance between sources and sinks of 24 Tg CH_4 (where 1 Tg
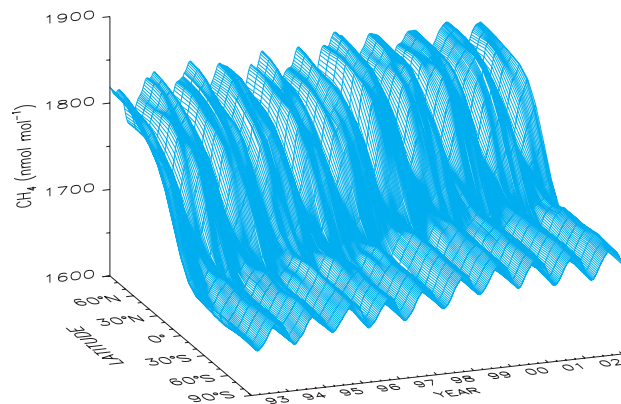

Figure 2.14. Three-dimensional representation of CH_4 mixing ratio versus latitude and time.
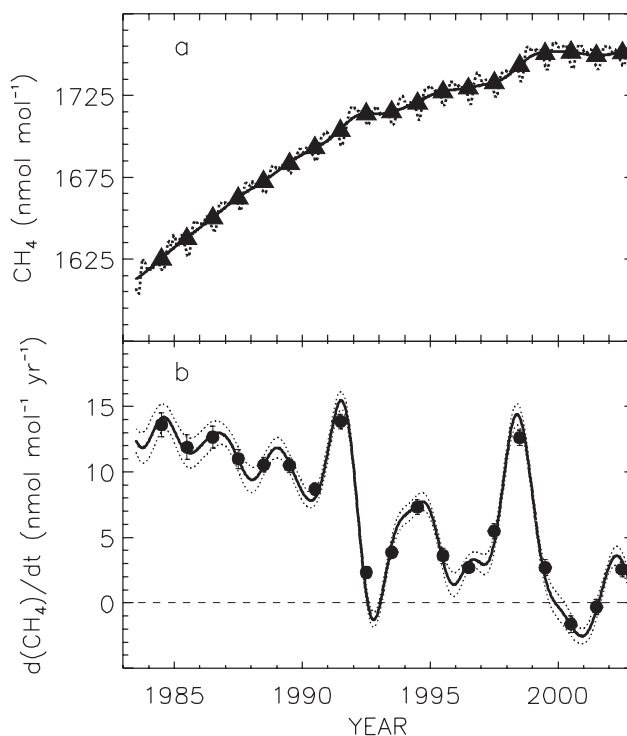

Figure 2.15. (a) Globally averaged methane mole fractions. The solid line is a deseasonalized trend curve. (b) Instantaneous global CH_4 growth rate. It is calculated as the derivative of the solid curve in 2.15a.

= 10^{12} g). *Dlugokencky et al.* [2001] attributed this to increased emissions from wetlands in the high-northern and southern-tropical latitudes resulting from warmer and wetter-than-normal conditions. *Walter* [1998] and *Walter and Heimann* [2000] used an adaptation of a process-based model that included soil-temperature and precipitation anomalies to calculate increased emissions for 1998 of 11.6 Tg CH_4 from wetlands north of 30°N and 13 Tg CH_4 for tropical wetlands compared to the average emissions calculated for 1982-1993. Nearly all (11.5 Tg CH_4) of

the tropical emission anomaly was in the southern tropics (equator to 30°S).

The observation of constant atmospheric methane during the four years between 1999-2002 was not expected, and it begs the question: Is the global CH_4 budget at steady-state? To answer this question CH_4 emission rates and sinks (and how they change with time) need to be quantified. Unfortunately, only the difference between these terms (the observed increase in the global CH_4 atmospheric burden) is known with reasonable certainty, and interannual variability in CH_4 growth rate may mask permanent changes in emissions from specific sectors. For example, during 1992 two emission sectors may have been affected: northern wetlands (as noted previously) and fossil-fuel emissions from the Former Soviet Union (FSU) when its economy collapsed. Decreased emissions from the FSU would have had a permanent affect on the latitudinal distribution of CH_4. In Figure 2.16, the change in the atmospheric CH_4 latitude gradient between mid-1980s and late-1990s is plotted. ΔCH_4 is calculated by first determining the difference in annual mean CH_4 mole fraction between each sampling site and the South Pole. These differences are then averaged for each site over two time periods: 1984-1986 (to represent the mid-1980s) and for 1997, 1999, and 2000 (to represent the late-1990s). Finally, each plotted symbol is the difference of the late-1990s average minus the mid-1980s average. Circles are based on the CMDL CH_4 data. The pattern of change, greatest at polar northern latitudes and decreasing towards the tropics, can only be explained by a permanent reduction in emissions from sources at high northern latitudes such as our proposed decrease from the FSU. To test this hypothesis, a 3-D transport model (Tracer Model, Version 3: TM3 [*Houweling et al.*, 2000]) was used to see if the changes in emissions as reported in Emissions Database for Global Atmospheric Research (EDGAR3) [*Olivier and Berdowski*, 2001; *Olivier*, 2002] are consistent with the observed change in ΔCH_4. A simulation was run at 4° latitude ×5° longitude resolution using assimilated, reanalyzed meteorological fields from the National Centers for Environmental Prediction for 1983-2000. Anthropogenic emission rates were from EDGAR3. Emissions distributions by source sector are available at 5-year intervals for 1980-1995. For other years in our simulation, global totals for combined sectors were scaled linearly to prescribe emissions for each sector. Emission rates from natural sources and CH_4 sinks, both constant throughout the simulation, were the same as in the work of *Houweling et al.* [2000], except that the ratio of emissions for bogs/swamps was as in the work of *Bergamaschi et al.* [2001]. Agreement between observed and modeled (triangles in Figure 2.16) ΔCH_4 is quite good. The change in emissions in EDGAR3 responsible for the change in CH_4 gradient is ~10 Tg CH_4 yr[1]. Therefore, it is likely that decreased CH_4 emissions from the fSU contributed to the zero growth in atmospheric CH_4 from 1999-2002. It is not believed that atmospheric CH_4 is at steady state. As economies in developing countries grow, so will their food production, energy consumption, and waste generation. Unless action is taken to reduce emissions elsewhere, this will result in increasing CH_4 emissions and increases in the atmospheric CH_4 burden.
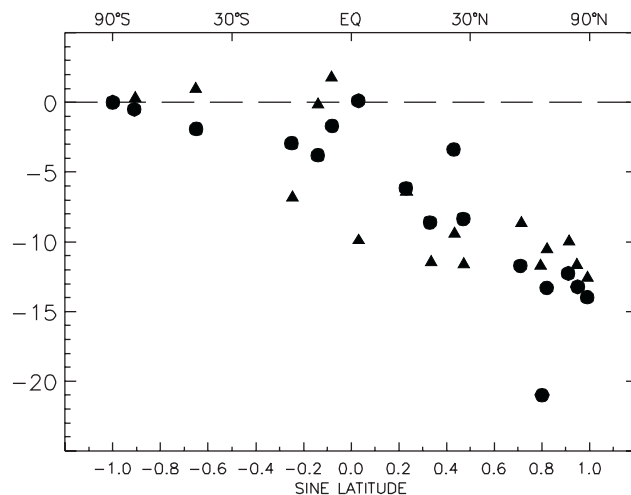

Figure 2.16. Change in atmospheric CH_4 latitude gradient between mid-1980s and late-1990s. ΔCH_4 is calculated by first determining the difference in annual mean CH_4 mole fraction between each sampling site and the South Pole. These differences are then averaged for each site over two time periods: 1984-1986 (to represent the mid-1980s) and for 1997, 1999, and 2000 (to represent the late-1990s). Finally, each plotted symbol is the difference of the late-1990s average minus the mid-1980s average. Circles are ΔCH_4 based on the CMDL CH_4 data. Sites were included only if they contain at least 1 full year of measurements in each 3-year averaging period. The site at $\Delta CH_4 = -20$ ppb is Shemya; its difference with South Pole decreased by ~10 ppb from 1991 to 1992 and then decreased by another 10 ppb after 1996 (except in 1998). The reasons for the second decrease are unknown. Triangles are ΔCH_4 calculated from results of a three-dimensional model simulation.

2.2.3. NITROUS OXIDE AND SF$_6$ MEASUREMENTS

Measurements of N_2O and SF_6 from all sites in the CMDL CCGG Cooperative Global Air Sampling Network continued during 2000 and 2001 on the Measurements of Atmospheric Gases Influencing Climate Change (MAGICC) analysis system. Annual mean mole fractions are given in Table 2.2 for N_2O and for SF_6.

2.3. CARBON MONOXIDE

2.3.1. MEASUREMENTS OF CARBON MONOXIDE

During 2002-2003 the study of the global distribution of CO in the lower troposphere continued. Surface measurements were made in air samples collected as part of the CMDL CCGG Cooperative Global Air Sampling Network and by in situ monitoring at BRW and MLO. The vertical profiling programs at Poker Flats, Alaska; Harvard Forest, Massachusetts; Molokai, Hawaii; and Rarotonga, Cook Islands, continued as part of the Measurement Of Pollution In The Troposphere (MOPITT) validation program. A revision of the CMDL CO reference scale and its application to all CCGG CO data was completed [*Novelli et al.*, 2003].

Flask measurements. Provisional annual mean CO mixing ratios for 2002 and 2003 are presented in Table 2.2. These values

are referenced to the revised CMDL CO scale (referred to as the CMDL/WMO 2000 scale [*Novelli et al.*, 2003]). The latitudinal distribution of atmospheric CO is shown as a three-dimensional representation of CO versus latitude and time in Figure 2.17.

Tropospheric CO shows a high degree of interannual variation (Figure 2.18). Most noteworthy is the 1997-1998 increase in CO that is widely believed to be due to biomass burning. The impact of large fires on global trace atmospheric constituents has become a subject of intense study [*Wotawa et al.*, 2001; *Langenfelds et al.*, 2002; *Duncan et al.*, 2003]. The CO zonal time-series (Figure 2.18) reflect the timing and locations of the 1997 and 1998 wildfires. CO was strongly enhanced in the low Southern Hemisphere beginning in late 1997. Fires in Indonesia burned agricultural areas, forests, and peat swamps in late 1997 [*Levine*, 1999]. In the high-latitude Northern Hemisphere, widespread burning of boreal forests in the summer and fall of 1998 consumed over 13 million hectares in Russia. The enhancement of CO north of 30ºN occurred rapidly during the fall months of 1998, leading to an early seasonal maximum. Extensive burning in Russia occurred again during 2002 and 2003, and higher levels of CO in the high northern latitudes were again found. The far western location of Shemya, Alaska, makes it sensitive to the transport of fire emissions from northeastern Siberia over the Bering Sea. Residuals from a smooth curve show the deviations from more typical years. Enhanced CO residuals in 1994, 1995, 1998, 2002, and 2003 all occurred during years of above normal burning (Figure 2.19).

In Situ Measurements. Quasi-continuous measurements of CO (three or four samples per hour) continued at BRW and MLO. The in situ record at BRW (Figure 2.20) shows the shallow summer minima in 1998 and 2003. Transport of CO from the 1998 eastern Russian fires is consistent with the high levels seen at BRW during 1998. Widespread burning occurred again in eastern Russia during 2003. The fire season began in early May and it is estimated that the area burned through August equaled that of the entire 1998 season (E. Kasischke, personal communication, 2003). The BRW flask samples and continuous measurements both show a weak summer drawdown in 2003 (Figure 2.20). The summer minimum in 2003 is shallower than observed in 1998, consistent with the early and intense fire season in 2003.
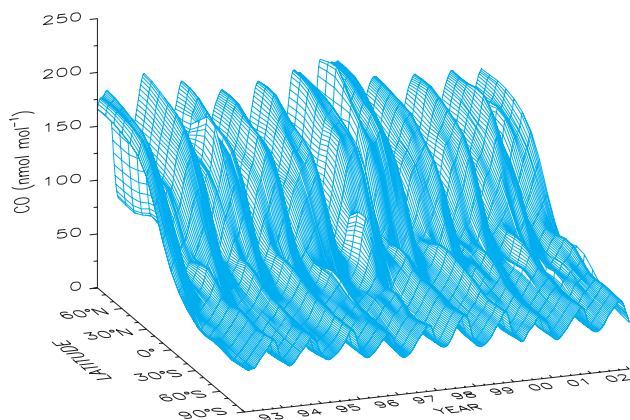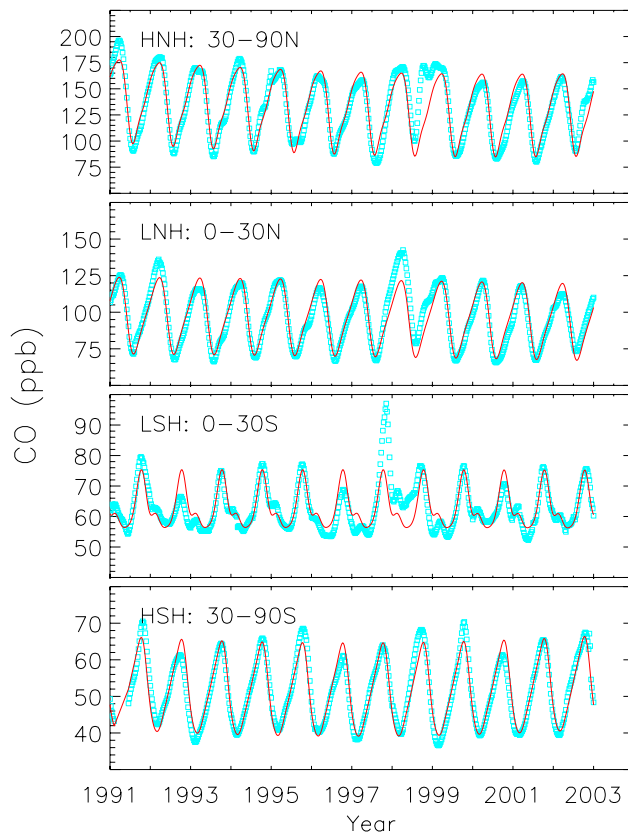

Figure 2.18. Zonal time series extracted from a smoothed, global surface created from the individual time series of 46 sites located in the marine boundary layer. Air samples were collected by the CMDL CCGG Cooperative Global Air Sampling program (Table 2.2). Symbols are the weekly zonal CO mixing ratios derived from the surface (Figure 2.17); the line is a function that represents the background signal [*Thoning et al.*, 1989].
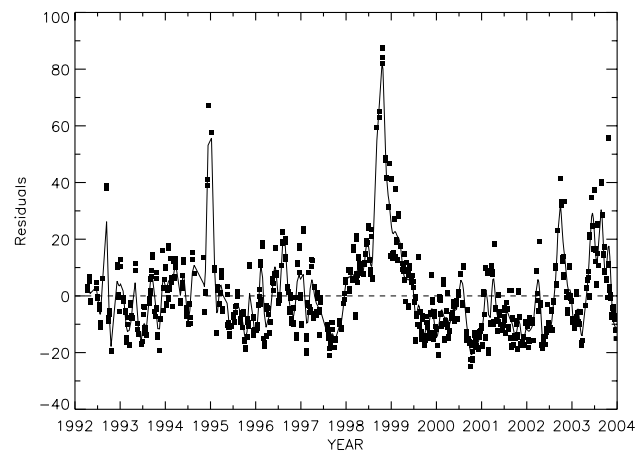

Figure 2.17. A smoothed representation of atmospheric CO mixing ratio versus latitude and time.

Figure 2.19. CO residuals from Shemya, Alaska, 1992-2003. The residuals are the difference between the function and the measured CO mixing ratios. The solid line is a smoothed fit to the data.
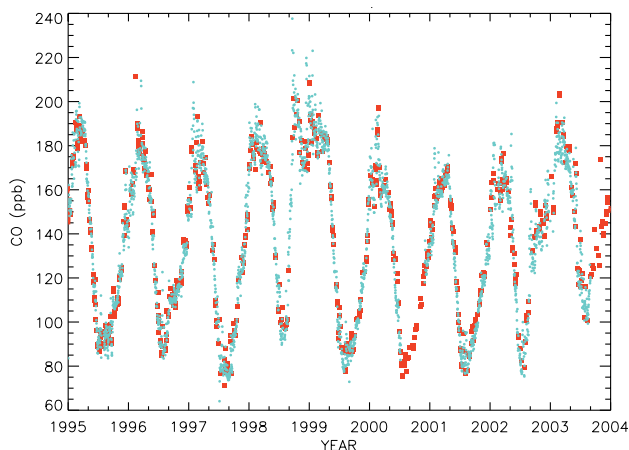
43

Figure 2.20. CO measured at BRW. Daily average CO determined in situ is shown as small green circles and the large red squares represent CO determined from flask air.

A WMO audit took place at MLO during August 2003. The audit was performed by the Swiss Federal Laboratory for Materials and Testing (EMPA) (www.empa.ch). They conducted quality-control experiments at the sites that make up the WMO GAW program (www.wmo.ch). The audit consisted of an onsite calibration of five EMPA transfer standards using the MLO in situ CO analyzer and its working standards. The results produced no surprises. At CO mixing ratios below 100 ppb, the CCGG measurements were 2-3 ppb lower than EMPA, while at greater mixing ratios the comparison showed better agreement. These results were similar to those obtained during a round-robin intercomparison of standards made in 2002 between EMPA and CMDL. The cause of the differences is still under investigation.

Vertical profiles. Funding from the National Aeronautics and Space Administration (NASA) Earth Enterprise System (formerly the Earth Observing System) continued to support measurements of the vertical profiles of CO and CH_4 from aircraft as part of the validation of the MOPITT instrument (http://www.atmosp.physics.utoronto.ca/MOPITT/home.html, see also Section 2.7). MOPITT is a nadir viewing, gas-filter correlation radiometer that determines the column distribution and total abundance of CO and column of CH_4. The CMDL CO vertical profiles conducted since 1999 were used to validate the space-based retrievals [*Emmons et al.*, 2004]. The aircraft data provide unique pictures of trace gas distributions (CO, CO_2, CH_4, H_2, N_2O, SF_6) above the boundary layer. For comparison to the MOPITT retrievals, the vertical profiles measured by CMDL are smoothed using the MOPITT averaging kernels. Because the aircraft reach altitudes of 7-8 km (350 mb) and MOPITT sees the entire tropospheric column, the aircraft data are extended to the tropopause using output from the Model for Ozone and Related Tracers (MOZART) three-dimensional (3-D) chemical transport model [*Emmons et al.*, 2004]. The satellite measurements generally agree with the aircraft profiles to within 10% (Figure 2.21).

2.3.2. CO REFERENCE GASES

The revision of the CMDL CO scale [*Novelli et al.*, 1991] was completed in 2002 [*Novelli et al.*, 2003]. The revision was necessary to correct for drift in the CMDL CO secondary and working standards. This experience showed that the scale must be maintained using several independent approaches. In response, a new set of 12 primary standards was first created in 260 ft^3 (7.4 m^3), high-pressure cylinders (Scott Marrin, Inc., Riverside, California). It will be determined if these larger cylinders exhibit lower drift rates than the previously used 150 ft^3 (4.3 m^3) tanks. The 12 standards, with target mixing ratios between 40 and 300 ppb CO, were calibrated against new gravimetric standards using a GC with an HgO reduction gas analyzer (RGA) (Trace Analytical, Menlo Park, California). They were also calibrated using a CO fluorescence technique that counts photons emitted after energetically excited CO relaxes to ground state [*Gerbig et al.*, 1996]. The technique is linear over a wide dynamic range (10^4). A Vacuum Ultraviolet Resonance Fluorescence detector (VURF) built by AeroLaser, Ltd. (Garmisch, Germany) was used. A U.S. National Institute of Standards and Technology (NIST) 9.6 ppm Standard Reference Material (SRM), diluted to atmospheric levels using a MKS Instruments, Inc., dilution-controller and MKS Instruments, Inc., mass-flow controllers, served as the reference gas. Initial results showed the two independent methods agreed to within 2%. However, it was later found that results from the dilution system were sensitive to its configuration, and a range of results (±5 ppb) could be obtained with different setups. CMDL standards calibrated on both the RGA and VURF were also measured at Max Planck Institute-Mainz using a manometric method. The intercomparison showed differences larger than expected based upon previous intercomparisons. Issues of CO standards and calibration will be addressed in 2004 by the WMO Scientific Advisory Group on reactive gases.

2.4. MEASUREMENTS ON TALL TOWERS

Measurements of CO_2 and other trace species continued to be made on a 447 m tall tower near Park Falls, Wisconsin (LEF) and a 505 m tall tower near Moody, Texas (WKT). The LEF site is a key element of the Chequamegon Ecosystem/Atmosphere Study (ChEAS) program that seeks to understand the processes that regulate the carbon balance in the temperate/boreal mixed forest surrounding the tower. CO_2 concentrations and CO_2 fluxes have been measured at LEF since October 1994. Measurement of CO, CH_4, N_2O, and SF_6 resumed at LEF in August 2003 after a 3-year hiatus, using an automated four-channel gas chromatograph (GC) [*Hurst et al.*, 1997, 1998]. The GC measurements provide an indicator of polluted air as described later in this section. The WKT site is located in a region of relatively dry grazing lands experiencing "woody encroachment," a process by which grasslands are gradually replaced by shrubs. Fire suppression is thought to contribute to woody encroachment in the southwest United States, and it has been proposed that woody encroachment may have been a significant sink for atmospheric CO_2 in recent decades [*Pacala et al.*, 2001]. CO_2 measurements began in February 2001 at WKT, and continuous CO measurements were initiated in June 2003.
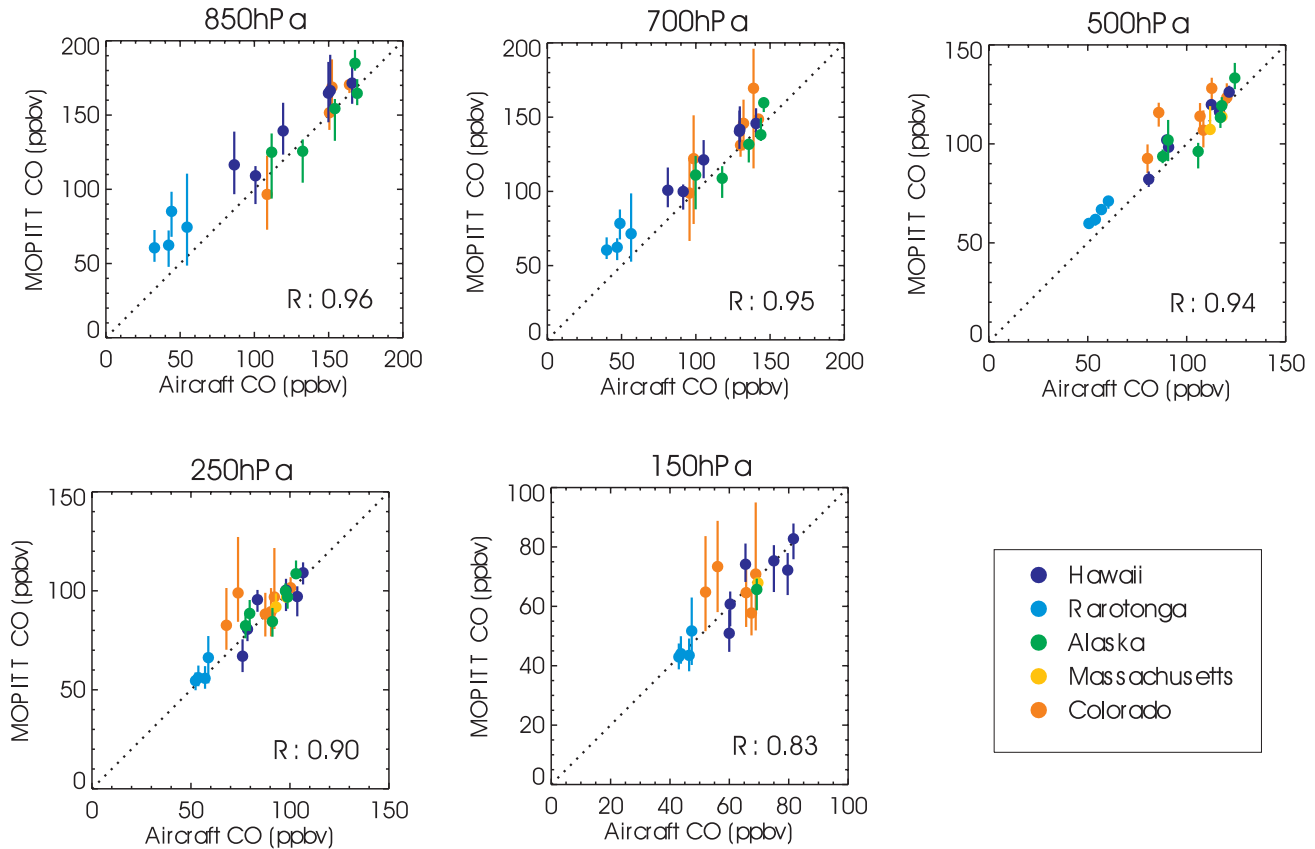
Figure 2.21. Comparison of aircraft CO with MOPITT retrievals (March 2000 to May 2001). "V3" is the most recent retrieval algorithm. The error bars represent the interquartile range for each MOPITT overpass. The dashed line is the 1:1 agreement; R is the Pearson correlation coefficient (adapted from *Emmons et al.*, 2004). The 250 hPa and 150 hPa panels compare the extrapolated profile with MOPITT.

A third tall tower site equipped for CO_2 and CO mixing ratio measurements was added in September 2003 near Argyle, Maine (AMT). The 120 m tower is 20 km south of the Howland AmeriFlux research site located in central Maine. The region is typical of forest industry land, with a patchwork of forest stands of various age and management classes. The climate is chiefly cold, humid, and continental with snowpack up to 2 m from December through March. The Howland AmeriFlux site includes three 30 m flux towers. Equipment for the AMT site was provided under a joint project led by researchers at Harvard University and the U.S. Forest Service. Trace gas measurements from AMT will play a key role in the CO_2 Budget and Rectification Airborne-Maine (COBRA-ME) study planned for 2004.

A major focus of the tower program over the last 2 years was to explore methods to calculate surface fluxes of CO_2 from mixing ratio data. Such fluxes are representative of large regions (i.e., approx. 10^6 km^2 [*Gloor et al.*, 2001]), and, therefore, are useful for understanding links between regional climate and the carbon balance of the vegetation.

Bakwin et al. [2004] examined the atmospheric budget of CO_2 at four temperate, continental sites in the Northern Hemisphere, including LEF. On a monthly time scale both surface exchange and atmospheric transport are important in determining the rate of change of CO_2 mixing ratio at these sites. Vertical differences

between the atmospheric boundary layer (ABL) and free troposphere (FT) over the continent are generally greater than large scale zonal gradients such as the difference between the FT over the continent and the marine boundary layer (MBL). Therefore, as a first approximation *Bakwin et al.* [2004] parameterized atmospheric transport as a vertical exchange term related to the vertical gradient of CO_2 between the ABL and FT and the mean vertical velocity from National Centers for Environmental Prediction (NCEP) reanalysis. Horizontal advection was assumed to be negligible in this simple analysis. Net surface exchange of CO_2 was then calculated from the CO_2 mixing ratio measurements at the four tower sites. The results provide estimates of surface exchange representative of a regional scale (~10^6 km^2). Comparison to direct, local scale (eddy covariance) measurements of net exchange with the ecosystems around the towers was reasonable after accounting for anthropogenic CO_2 emissions within the larger area represented by the mixing ratio data (Figures 2.22 and 2.23).

In a similar study (B. Helliker et al., manuscript in preparation, 2004) monthly averaged flux and mixing ratio data for water vapor at LEF were used to obtain estimates of vertical velocity exchange between the ABL and FT. These vertical velocity estimates were used to calculate regionally representative, monthly CO_2 surface fluxes for the site that again were in reasonable accord with local-scale eddy covariance fluxes.
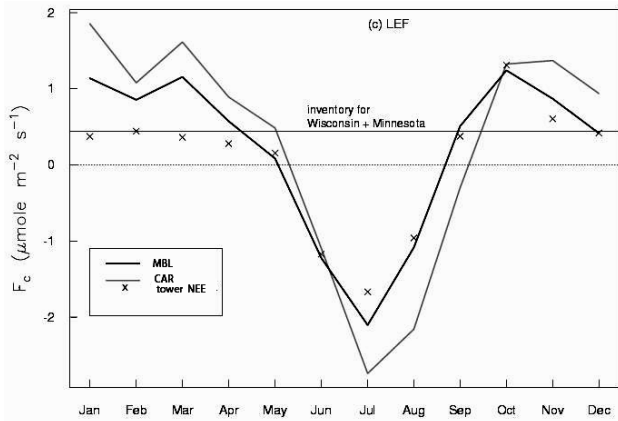
Figure 2.22. Regional CO_2 flux estimates at LEF from the ABL budget method from the work of *Bakwin et al.* [2004] (lines), and local fluxes measured at the towers by eddy covariance methods (×). CO_2 in the free troposphere over the tower was estimated either from MBL data (black line) or aircraft data from 5 km over Carr, Colorado (CAR; gray line). Thin horizontal lines indicate inventory estimates of fossil fuel emissions of CO_2 for Wisconsin and Minnesota.
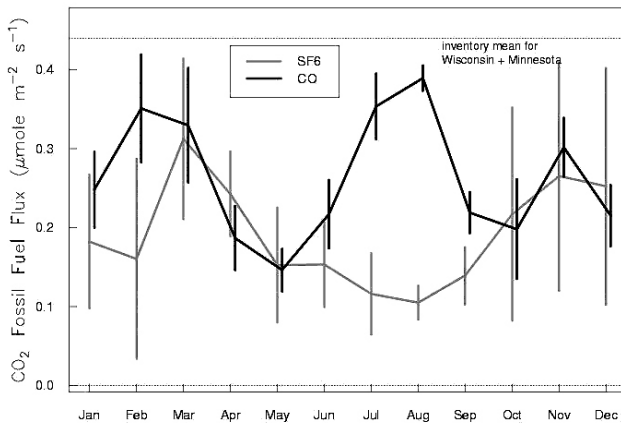

Figure 2.23. Regional fossil fuel flux of CO_2 at LEF estimated from CO and SF_6 data using the ABL budget method. Measurements of SF_6 were started in mid-1997. Data are averaged for 1998-2001, and error bars show one standard deviation of the mean across years. Annual mean fossil fuel emissions from inventory estimates (dashed horizontal lines) were calculated by multiplying the human population density by the national per capita emissions [*Marland et al.*, 2002].

The results of these studies indicate that it is feasible to measure surface fluxes of CO_2 on a regional scale (~10^6 km^2) by using measurements of CO_2 mixing ratios if horizontal and vertical advection can be estimated. The parameterizations in these studies were necessarily rough because, at present, sufficient data do not exist to enable a more accurate representation of horizontal and vertical advective exchange. Also, proxy data (such as the marine boundary layer) were used to estimate CO_2 in the FT. A network of tower sites and frequent aircraft vertical profiles separated by several hundred km, where

CO_2 is accurately measured, would provide data to estimate horizontal and vertical advection and, hence, provide a means to derive net CO_2 fluxes on a regional scale. At present CO_2 mixing ratios are measured with sufficient accuracy relative to global reference gas standards at only a few continental sites. The results of *Bakwin et al.* [2004] and (B. Helliker et al., manuscript in preparation, 2004) also confirm that flux measurements from carefully sited towers capture seasonal variations representative of large regions.

The tower program made a key contribution to the CO_2 COBRA experiment. During COBRA-2000 a regional budget study was carried out in the area around LEF, and COBRA-2003 flights were made over and around WKT. Flight and tower data from COBRA-2000 were used in a detailed study of methodologies to constrain regional CO_2 budgets over North America [*Gerbig et al.*, 2003a, 2003b]; (J.C. Lin et al., manuscript in preparation, 2004). *Bakwin et al.* [2003] used data from LEF and flights above it to examine sampling strategies to define CO_2 column amounts by discrete (flask) sampling. Data from COBRA-2003 are currently being analyzed. A further flight series is planned for 2004 with a focus in the region around AMT.

GC measurements of CO, CH_4, N_2O, and SF_6 resumed in August 2003 at LEF. Measurements are made hourly on air drawn from 30, 76, and 396 m above the ground. The GC is calibrated hourly using low and high calibration tanks tied to the reference scales established and maintained at CMDL. The plan is to resume measurement of several halogenated species (CFC-11, CFC-12, CFC-113, methyl chloroform, and carbon tetrachloride) in early 2004. Hourly measurements complement the weekly CCGG flask measurements allowing variability analysis on shorter timescales. Daily averaged concentrations of CO, CH_4, N_2O, and SF_6 measured at 76 m during September 2003 illustrate the synoptic variability captured by the GC measurements (Figure 2.24). Back trajectories show how the synoptic meteorology drives the day-to-day variability in trace gas mixing ratios (Figure 2.25). Air from the north and west is associated with background concentrations (1-5, 14-16, 19-20, 23-24 September), while transport from the south brings elevated pollutant levels (10-13, 17-18, 21-22 September) and higher variability. In the future these measurements will be used in an inverse modeling framework with high resolution transport models to diagnose the surface source distribution of these greenhouse gases.

2.5. DATA INTEGRATION (GLOBALVIEW)

In August 2003 the eighth annual update of GLOBALVIEW-CO_2 was made freely available from the GLOBALVIEW Web site (http://www.cmdl.noaa.gov/ccgg/globalview/index.html). GLOBALVIEW is a product of the Cooperative Atmospheric Data Integration Project and is coordinated and maintained by CCGG. *GLOBALVIEW-CO_2* [2003] and *GLOBALVIEW-CH_4* [2001] are designed to enhance the spatial and temporal coverage of global atmospheric observations of carbon dioxide and methane. The GLOBALVIEW products are derived from measurements made by many international laboratories and are specifically intended as a tool for use in carbon cycle modeling studies. To facilitate use with models, the measurements are processed (smoothed, interpolated, and extrapolated) resulting in
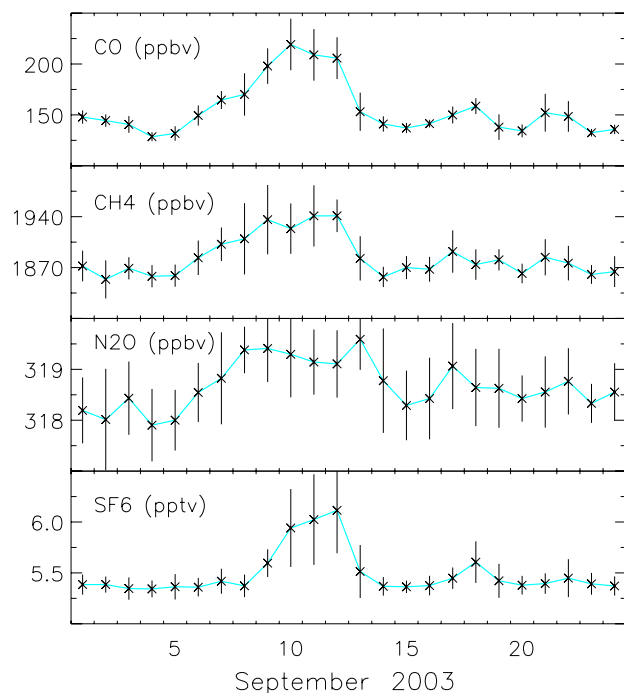
46

Figure 2.24. Daily averaged concentrations (24 1-hour values) of CO, CH_4, N_2O, and SF_6 measured at 76 m during September 2003 at the LEF tower. Error bars represent the standard deviation of the daily mean.
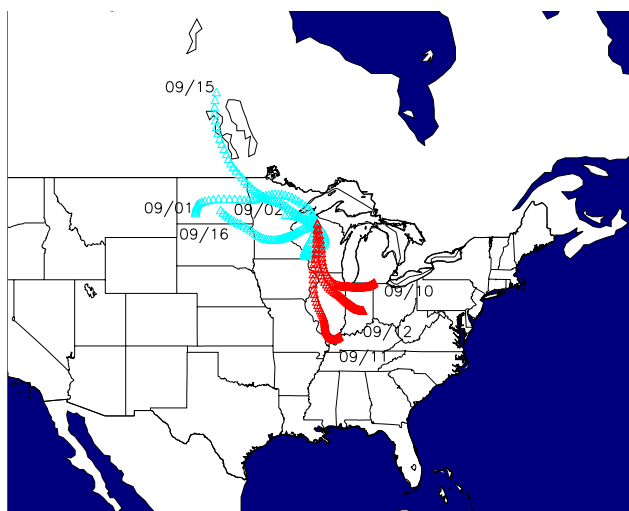

Figure 2.25. Forty-eight hour back trajectories generated by the NOAA ARL Hysplit-4 AVN model [*Draxler and Hess*, 1997] originating at 500 m above the ground surface at 1800 UTC (noon local time). The back trajectories are labeled with the day they arrived at the tower with blue designating clean air and red representing days with elevated greenhouse gas concentrations.

extended records evenly incremented in time. The data products include synchronized smoothed time series derived from continuous and discrete land-surface, ship, aircraft, and tall tower

observations along with summaries of seasonal patterns, diurnal patterns (where relevant), sampling time-of-day (where available), and atmospheric variability. They also include the derived marine boundary layer (MBL) reference matrix used in the data extension process [*Masarie and Tans*, 1995], uncertainty estimates, and extensive documentation.

GLOBALVIEW-CO$_2$ [2003] includes 202 extended records derived from observations made by 23 laboratories from 15 countries (Figure 2.26). Data updates through 2002 (where available) were used to derive the product. Several new data sets were added in 2003 including discrete surface measurements from Begur, Spain (Laboratoire des Sciences du Climat et de l'Environnement (LSCE), France) and Summit, Greenland (CMDL); semi-continuous surface measurements from Fraserdale, Ontario, Canada (Meteorological Service of Canada (MSC)) and Pallas, Finland (Finnish Meteorological Institute (FMI)); and semi-continuous measurements from WKT. Also in 2003, participants of the Cooperative Atmospheric Data Integration Project agreed to change the GLOBALVIEW-CO$_2$ release policy by making a single complete version of the product freely available to everyone. Prior to 2003 the policy called for two versions: a complete version available to all data contributors and a second version available to all others excluding the most recent 3 years of extended values.

The GLOBALVIEW data products continue to be an important resource to the carbon cycle science community. In 2002 and 2003, 2324 FTP requests (97 per month) for GLOBALVIEW-CO$_2$ were made from 44 countries. GLOBALVIEW-CH$_4$ received 789 FTP requests (33 times per month) during this same 2-year period. Since their first release in 1996 and 1999, GLOBALVIEW-CO$_2$ and GLOBALVIEW-CH$_4$ were cited in 66 reviewed journal articles (source: ISI Web of Science).

Assessing the level of comparability among measurements made by different laboratories continues to be a primary focus of this activity. The challenge is to ensure spatial and temporal patterns among observations from the cooperative global network arise from CO$_2$ sources and sinks, as modified by atmospheric mixing and transport, and are not due to inconsistencies among internal calibration scales and potential systematic errors introduced when sampling the atmosphere. Current scientific objectives require a global network precision of 0.1 μmol mol^{-1} among Northern Hemisphere observations and 0.05 μmol mol^{-1} among Southern Hemisphere observations [*WMO*, 1981]. Data sets that cannot be integrated with a more extensive global cooperative network of observations have limited value. Demonstrating that a data set is consistent with others to the levels necessary to address carbon cycle issues greatly improves the value of the data and strengthens the measurement laboratory's program.

Ongoing flask air intercomparison (ICP) experiments continue to be an essential tool for assessing the comparability of atmospheric measurements. In these experiments, participating laboratories directly compare measurements from the same atmospheric sample collected weekly in glass containers [*Masarie et al.*, 2001]. Questions addressed include: (1) How consistent are our observations with observations made using independent methods or by other laboratories? (2) How can ICP results be used to improve our experimental methods? (3) At what confidence level can we merge data from these two programs?
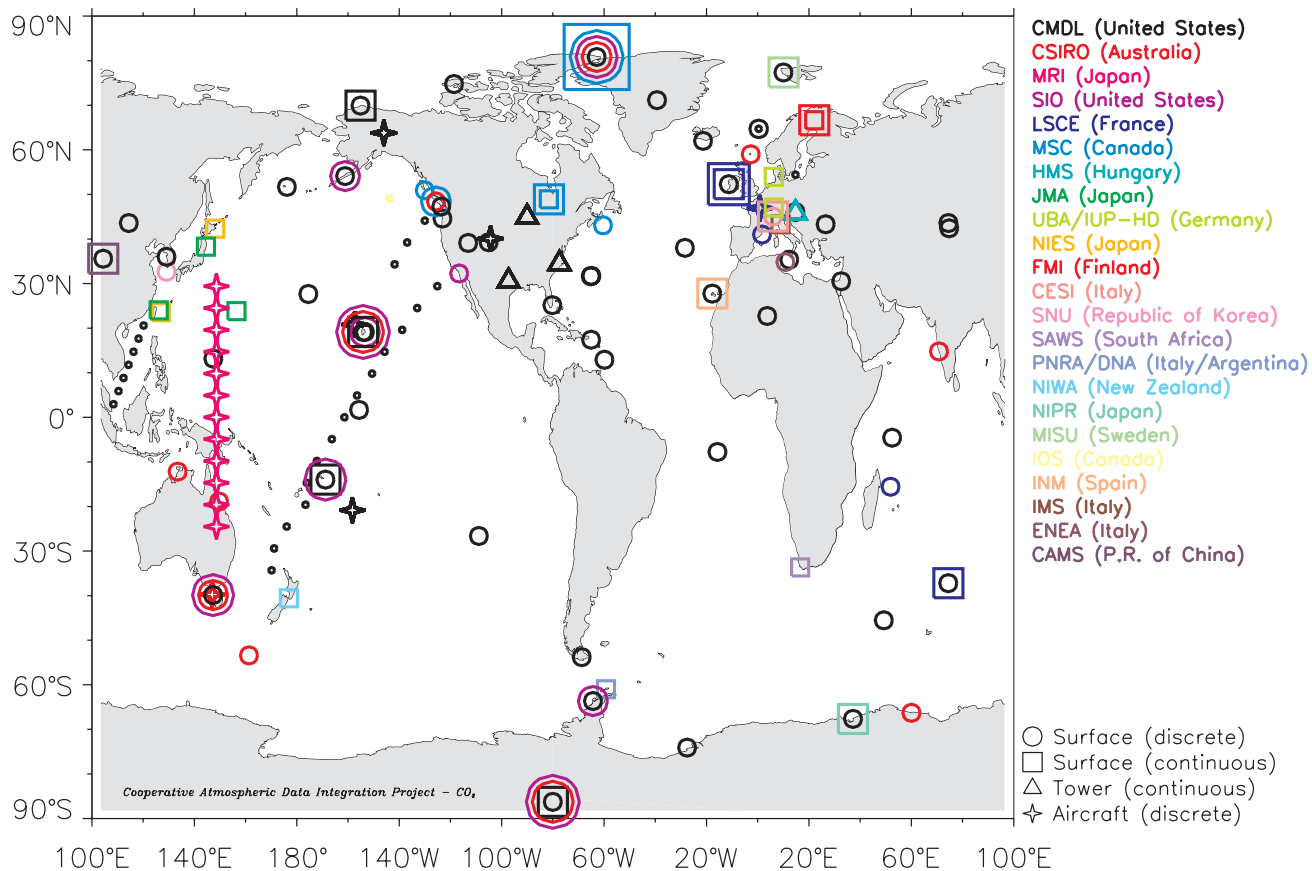
Figure 2.26. Locations of observations used to derive GLOBALVIEW-CO$_2$, 2003.

We use the following strategies to improve the effectiveness of the ICP experiments. First, the ICP is viewed as an additional means of assessing the quality of the observations. Observed differences motivate further scrutiny of analytical methods and encourage the design of additional experiments that might independently determine the cause of discrepancies [*Tans et al.*, 2002]. Second, the ICP activities are ongoing in order to establish and maintain comparability throughout the observing period. Third, weekly comparisons that can be analyzed routinely become our goal and this improves our ability to link observed changes in the ICP results with changes in laboratory procedures. Fourth, supporting comparisons are included that can be used to narrow possible causes when differences are observed and to assess the level of comparability of observations made at other locations by CMDL and the participating laboratory. Additionally, our goal is to maintain the shortest possible link to internationally recognized absolute calibration scales (where they exist). Finally, the impact of the ICP activity on daily operations is minimized using automation. Advanced data management tools allow CCGG to analyze, process, and automatically exchange ICP data with the participating laboratory. ICP results are routinely and automatically summarized and posted to a restricted Web site. Participants are then electronically notified when an update becomes available. Timely feedback improves the likelihood that potential problems are detected early.

Ongoing flask air ICP experiments with the Commonwealth Scientific and Industrial Research Organization (CSIRO), Australia, and MSC continued. In 2003 a new flask air ICP experiment was established with the Max Planck Institute of Biogeochemistry (MPI-BGC) using weekly samples collected on a tower in Oschenkopf, Germany. Work is underway to establish a flask air ICP experiment with LSCE using weekly samples collected at Mace Head, Ireland. Both MPI-BGC and LSCE are key participants in the Airborne European Regional Observations of Carbon Balance (AEROCARB), an European Union-sponsored multi-national project designed to improve understanding of the carbon budget in Europe. These experiments will provide ongoing information on the comparability of carbon cycle trace gas measurements made by CMDL and major European measurement laboratories.

2.6. A WEB-BASED INTERACTIVE ATMOSPHERIC DATA VISUALIZATION TOOL: NEAR REAL-TIME ACCESS TO DATA FROM THE CMDL CCGG OBSERVING NETWORK

CCGG plans to greatly expand its observational network in coming years. Intensive aircraft and tall tower sampling in North America represents our commitment to NACP. Continued expansion of the CMDL CCGG Cooperative Global Air

Sampling Network is expected to improve data coverage in under-sampled regions of the world. These proposed expansions will increase, by an order of magnitude, the volume of data currently managed. A recent assessment of the current data management strategy and quality-control procedures focused on the ability to maintain the high standard required for data produced by this laboratory under the expected expansion. Several limitations of the current strategy were identified, resulting in modifications that improve the ability to manipulate and probe data generated by the flask, aircraft, tower, and observatory programs. A Web-based interactive atmospheric data visualization (IADV) tool intended to improve the ability to quickly assess the quality of a growing volume of data (Figure 2.27 and http://www.cmdl.noaa.gov/ccgg/iadv/) was introduced. The tool is also designed to better serve users outside CCGG including students, educators, the press, business, and policy makers as well as the scientific research community. To achieve these objectives the IADV tool: (1) accesses the operational database in order to make all data available including the most up-to-date measurements; (2) centralizes access to a growing library of graphing tools developed within CCGG; (3) requires minimal maintenance; (4) ensures flexibility and adaptability; (5) provides an environment in which users can easily manipulate the data and prepare custom graphs that can be saved in a variety of formats; (6) uses simple development tools that do not require users to download plug-ins, add-ons, or updates; (7) performs consistently on a variety of computers and browsers; and (8) serves users with typical internet access speeds. Additionally, because users can view near real-time data that have not yet been screened for calibration or experimental problems, these "preliminary" data are clearly identified and their limitations are explicitly stated.

The IADV Web site was launched in May 2003. Since then, the site has been visited more than 2250 times (~250 per month) from 49 countries. The site currently provides details on each sampling location; acknowledges our cooperating and sponsoring agencies; presents graphs depicting time series, average seasonal patterns, vertical profiles, south-to-north latitudinal distributions, global surfaces, and flask in situ comparisons; and enables users to create custom graphs using data from multiple sites and multiple trace gases. To maximize the usefulness of the site, thousands of the most frequently requested graphs (Figure 2.28) are routinely and automatically prepared. This ensures that the majority of requests are displayed with no delay. Advanced graphing functions allow users to select any number of data sets and manipulate, compare, and plot data in whatever manner they choose. Custom requests take several seconds to process as data are extracted from the database and the graph prepared using user-defined preferences.

The IADV Web site is not yet fully functional and will continue to evolve with time. Future plans include expanding the selection of prepared graphs, providing the ability to highlight a region on the global map, and displaying all flask, aircraft, tower, and observatory data derived from within the region. Additional functionality will be added as users and project leaders discover new ways to explore and evaluate the CCGG observations.

2.7. AIRCRAFT SAMPLING PROGRAM

Funding provided for NACP allowed CMDL to add six vertical profile sites to the existing CMDL CCGG Cooperative Global Air Sampling Network (Table 2.7). Using funds from the NASA Earth Enterprise System and working in collaboration with the MOPITT science team, CMDL continues to collect and analyze samples at the five MOPITT sampling locations (Table 2.7). Also, CMDL continues to participate in the Large Scale Biosphere Atmosphere (LBA) experiment collecting air samples near Santarem and Fortaleza, Brazil. Samples are collected using the Automated Air Sampling System (version 2.0). The Automated Air Sampling System version 2.0 is used aboard
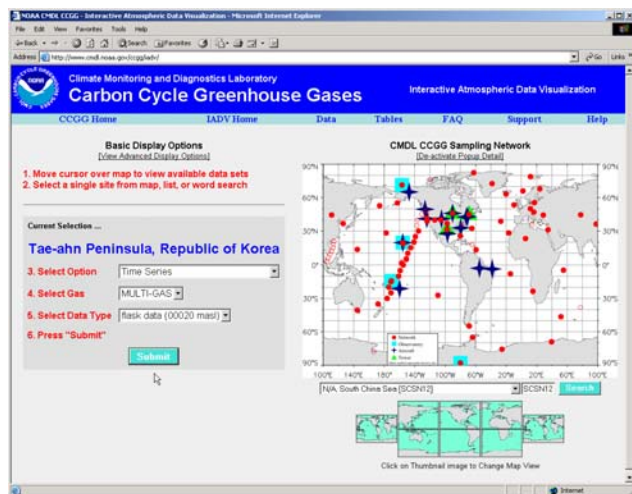

Figure 2.27. Interactive Atmospheric Data Visualization (IADV) home page. Web address: http://www.cmdl.noaa.gov/ccgg/iadv/.
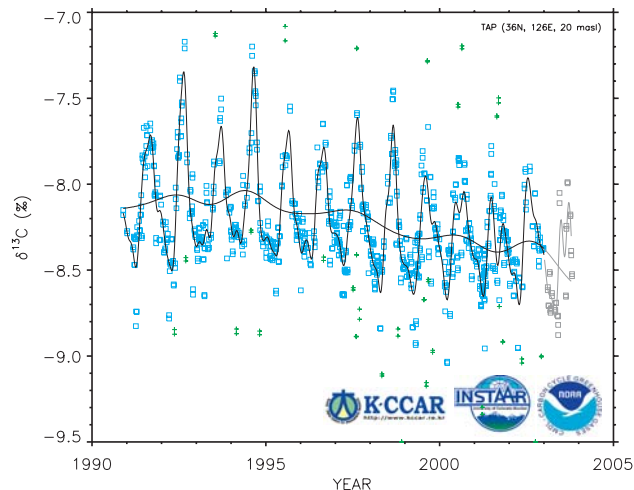

Figure 2.28. Graph produced using the IADV Web site on 17 January 2004. Cooperating agencies are identified in the lower right portions of the graph (Korean-China Centre for Atmospheric Research (K-CCAR), INSTAAR, and NOAA). Preliminary data, and the curves derived from preliminary data, are clearly identified in gray.

Table 2.7. CMDL Vertical Profile Sampling Sites

Site	Latitude	Longitude	Maximum Altitude (km)	Environment	Start Date	Program
Carr, Colorado	40.9ºN	104.8ºW	7.9	NH background continental	1992	NACP MOPITT
Estevan Point, British Columbia	49.6ºN	126.4ºW	5.5	NH background oceanic	2002	NACP
Fortaleza, Brazil	3.5ºS	38.3ºW	4.3	SH background oceanic	2000	LBA
Harvard Forest, Massachusetts	42.5ºN	71.2ºW	7.6	NH background continental	1999	NACP MOPITT
Molokai, Hawaii	21.4ºN	157.2ºW	7.6	NH background oceanic	1999	MOPITT
Park Falls, Wisconsin	46.0ºN	90.3ºW	3.8	NH background continental	2002*	NACP
Poker Flats, Alaska	65.1ºN	147.5ºW	7.3	HNH background continental	1999	MOPITT
Raratonga, Cook Islands	21.2ºS	159.8ºW	6.1	SH background oceanic	2000	MOPITT
Santarem, Brazil	2.9ºS	55.0ºW	3.7	SH background continental	2000	LBA
Sinton, Texas	27.7ºN	96.9ºW	7.6	NH background oceanic	2003	NACP
Summerville, South Carolina	32.8ºN	79.6ºW	7.6	NH background oceanic	2003	NACP
Trinidad Head, California	41.1ºN	124.2ºW	7.6	NH background oceanic	2003	NACP
Worcester, Massachusetts	43.0ºN	70.6ºW	7.6	NH background oceanic	2003	NACP

*Restart date after gap in record.

chartered aircraft to collect air samples at a frequency of about once per month at all sites. Regular sampling builds time series that define the trends and seasonal cycles of CO_2, CH_4, CO, H_2, N_2O, and SF_6. An example for CO_2 is shown in Figure 2.29. These data, as well as site information, can be found on CMDL's Web site (http://www.cmdl.noaa.gov/ccgg/iadv).

The Automated Air Sampling System version 2.0 consists of two suitcases, a display module, electrical cables, and hoses. The

Figure 2.29. Representative CO_2 time series from Carr, Colorado, binned for each 2000 ± 1000 m altitude.

first suitcase, the Programmable Flask Package (PFP), contains 17 or 20 glass sampling flasks and a controller. The second suitcase, called the Compressor Package (CP), contains the power supply and the compressors. The system can be installed quickly on any aircraft provided there is room to stow the cases and a clean air intake is set up. In most cases, a sampling inlet is created on a modified pilot window. A barometric pressure sensor was added to this sampling system in the past year. This addition provides a much needed check on the correct execution of the intended flight plan. After a sample flight is finished, the CP suitcase remains on site and the batteries are recharged to prepare for the next flight. The PFP suitcase is shipped back to CMDL for automated air sample analysis. CMDL's analytical system measures each flask for CO_2, CH_4, CO, H_2, N_2O, and SF_6. INSTAAR's analytical system performs isotopic analysis of CO_2 using mass spectrometry. Currently, samples from the MOPITT sites are not analyzed for isotopes.

Field use and laboratory testing of the Automated Air Sampling System version 2.0 resulted in documented needs for design improvements. Design efforts, using the documented repair history of version 2.0, culminated in the design and production of the Automated Air Sampling System version 3.0. The design goals were to improve ruggedness through weight reduction, decreasing from 17 or 20 flasks to 12 flasks; to improve repair efficiency by increasing the accessibility of manifolds, actuators, and flasks; to upgrade the electronics by consolidating all printed circuit boards into one controller board; and to improve system communication, both sample system to sample system, and sample system to other instrumentation.

Over the past year, CMDL has planned and started an expansion of the vertical profile network on the North American continent. More than 70 Automated Air Sampling System version 3.0 PFPs and 15 Programmable Compressor Packages (PCPs) are in production. Our sample preparation and analysis facilities are expanding to meet the new demand, and plans are under way to locate and start air sampling at over 20 new sites in North America over the next 3 years (Figure 2.30). In addition, plans are in place to add at least 10 vertical profile sampling sites outside of North America beginning with sites in eastern Asia.
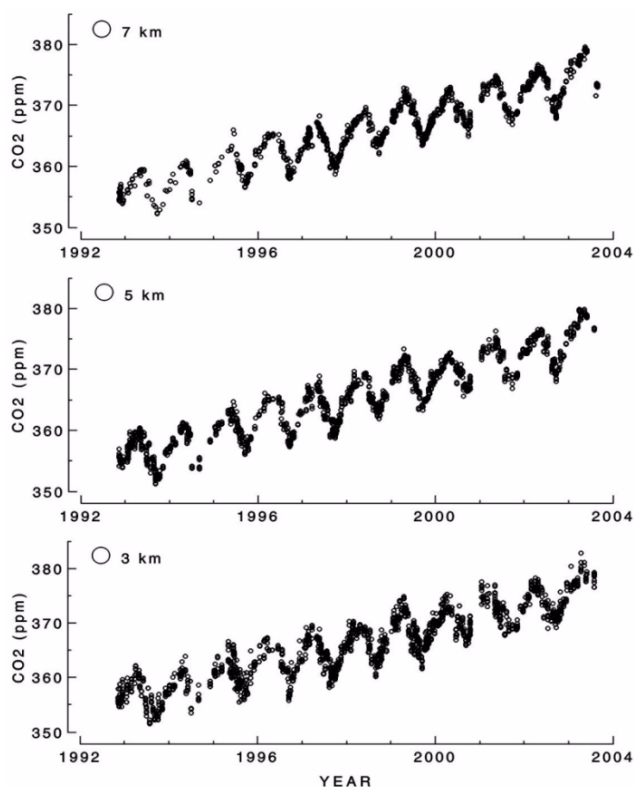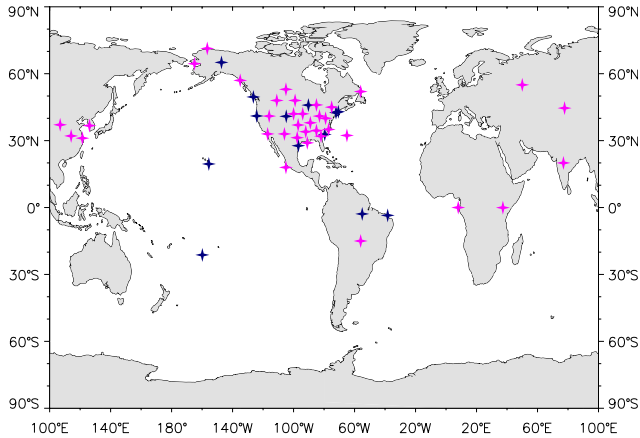
50

Figure 2.30. Locations of the CCGG vertical profile sites. Current sites are shown in dark blue and planned sites (2007) are shown in magenta.

2.8. ATMOSPHERIC TRANSPORT MODELING AND MODEL-DATA SYNTHESIS

Inherent in observations from the CMDL CCGG Cooperative Global Air Sampling Network is information about the spatial and temporal variability of the sources and sinks of measured atmospheric species. Using an atmospheric transport model and inverse technique, the observations may be used to estimate surface fluxes and their uncertainties. The problem is made particularly challenging by the fact that some regions are not well constrained by observations, leading to unrealistic, noisy solutions for those regions. This complication has generally been treated by the addition of a priori information in the estimation process. In addition, transport models are not always able to accurately represent transport processes at specific sites, resulting in estimation errors. This is particularly true for sites where the local meteorology depends on sub-grid scale events, such as sea breezes or sites sampling plumes emanating from local urban areas.

Modeling efforts in the CCGG are currently focused on the development of improved inversion methods that address the problems described previously and applications of inverse techniques that take maximal advantage of the wealth of observations collected by the CMDL CCGG Cooperative Global Air Sampling Network. In the near future relatively dense sampling over North America as part of NACP will make it possible for fluxes to be estimated on sub-continental scales for this region, and intensive efforts to develop the tools and techniques for this are in progress at CCGG. Specific research projects are described in the following sections.

2.8.1. THE FIXED-LAG KALMAN SMOOTHER

An important aspect of estimating fluxes for atmospheric trace species with long residence times is that emissions at a particular time have the potential to affect the predicted concentration at all subsequent times. This implies that transport response, or basis functions, must be propagated indefinitely, a computationally prohibitive task for a reasonable distribution of source regions

and monthly resolution of fluxes over periods of years to decades. Basis functions are commonly calculated for several years and extrapolated beyond that. A more computationally efficient method is to transport pulses forward in time only until they become sufficiently dispersed by transport. This is possible because most of the information about the spatial and temporal structure of carbon fluxes is captured during the first 4-6 months of the propagation of the response function pulses. Therefore, the propagation of the basis functions is limited to 4-6 months and the solution flux estimates and uncertainties for the previous 4-6 months are obtained using a framework based on fixed-lag Kalman smoothing [*Gelb*, 1974; *Kalman*, 1960]. After the final flux estimates are made for a particular month they are incorporated into the background state of the model by using the calculated response function fields. The background CO_2 abundances are then propagated forward in time, and all rows of matrices and vectors are shifted to make room for the new month's transport and observational information. In this way new observations may be added to the inversion while keeping the size of the problem the same at each time step. Tests comparing our time-dependent technique with the standard batch method (that solves for all regions and time steps at once, potentially involving very large matrix operations) have shown nearly identical results when response functions are transported for only several months rather than for several years (L. Bruhwiler et al., manuscript in preparation, 2004).

We recently developed a technique that enables the fixed-lag Kalman smoother to correctly propagate estimation uncertainties and covariances forward in time. Previously the uncertainty on the final estimate for a particular time step was not taken into account in estimating fluxes for subsequent months. Our new covariance propagation technique corrects these omissions with the net result of increased flux estimate uncertainties relative to the standard batch approach. The difference between the fixed-lag Kalman smoother and the batch uncertainty estimates decreases as the number of months that the basis functions are transported increases (Figure 2.31).

Figure 2.32, shows global carbon flux estimates and their uncertainties for 1980 through October 2003, obtained using the fixed-lag Kalman smoother. For 2003, only observations from a subset of the CMDL network sites were available at the time of publication. These estimates will be updated as more data become available.

2.8.2. MODELING ATMOSPHERIC TRANSPORT WITH A NESTED-GRID MODEL: IMPLICATIONS FOR INVERSIONS OF TRACE SPECIES

The state-of-the-art Transport Model 5 (TM5) (M.C. Krol et al., manuscript in preparation, 2004) offers the option of online, two-way nesting of (multiple) fine resolution grids within the global model domain. The TM5 model bridges the gap between regional models with limited domains and global models with limited resolution. It is ideally suited to a detailed study of the United States' CO_2 budget in both space and time ensuring the consistency with long-term global observations. Figure 2.33 shows the current model configuration with a global resolution of 6° longitude by 4° latitude and two nested regions over North America with grid sizes of 3° longitude by 2° latitude, and 1°
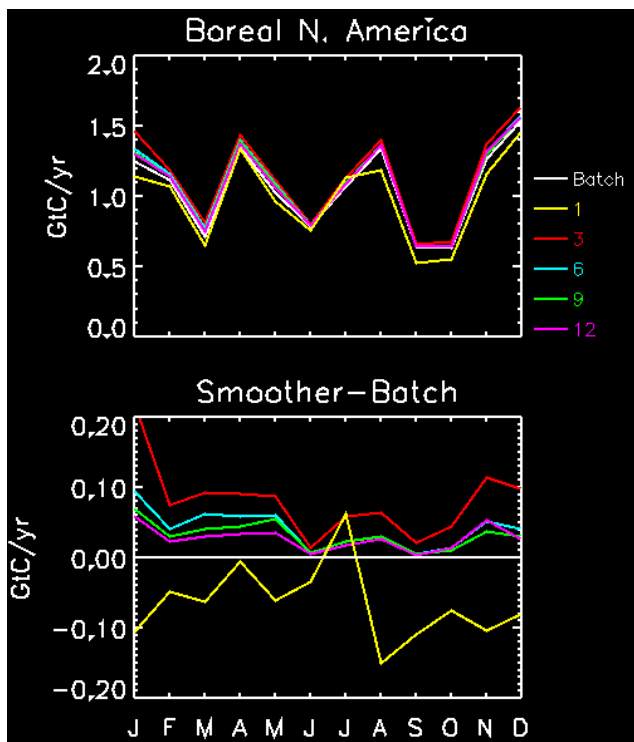
Figure 2.31. Monthly flux estimate uncertainties for Boreal North America for the third year in a 5-year test inversion. The white curve represents uncertainties from the batch calculation that uses all 5 years of data and basis functions transported for 5 years in a single inversion step. The yellow, red, blue, green, and magenta lines represent uncertainties obtained using the fixed-lag Kalman smoother and keeping 1, 3, 6, 9, and 12 month's worth of transport. The bottom plot shows the difference between the batch calculation and the Kalman smoother results. Note that the batch uncertainties are expected to be the lowest since all of the data are used to obtain the solution. Note also that the uncertainties approach the batch solution as more transport information and data are used to obtain each month's solution. Transporting basis functions for only 1 month incurs large differences from the batch. The uncertainties for the 1-month case are also unrealistic since the uncertainties are smaller than for the batch solution.

Figure 2.32. Total land (top) and ocean flux (bottom) estimates and 1 sigma uncertainty limits. The red curves use meteorological analyses from the National Centers for Environmental Prediction, while the white curves use meteorological analyses from the European Center for Medium-Range Weather Forecasting (ECMWF). The figures show an apparent bias between the two sets of analyzed wind fields. Note that meteorological fields for 2003 were unavailable, therefore, the windfields for 2002 were used for this year. Note also that the observations for 2003 are limited to sites operated by CMDL. This figure will be updated as more meteorological analyses and measurements become available. The large anomaly during 1998 was mainly due to decreased uptake by the global biosphere.

longitude by 1° latitude, respectively. The fine grid over the United States allows optimal use of the relatively dense CMDL CCGG Cooperative Global Air Sampling Network and minimizes representation errors for the many new continental sites that will be part of NACP [*Wofsy and Harriss*, 2002].

Three major steps towards high-resolution CO_2 inversions were taken in 2003. First, a set of transport fields at the appropriate resolutions based on the ECMWF weather forecast model was prepared for 2000-2003. In the near future, meteorology from the new ECMWF 40-year reanalysis (1959-2000) will be available, and nested grids up to ~40 × 60 km will be possible, still in a global model framework. TM5 was installed on NOAA's high-performance computing platform "Jet." Second, a set of base functions was calculated for every CMDL flask sample taken since 1 January 2000 in the previously mentioned model setup. This set will form the basis for high-resolution
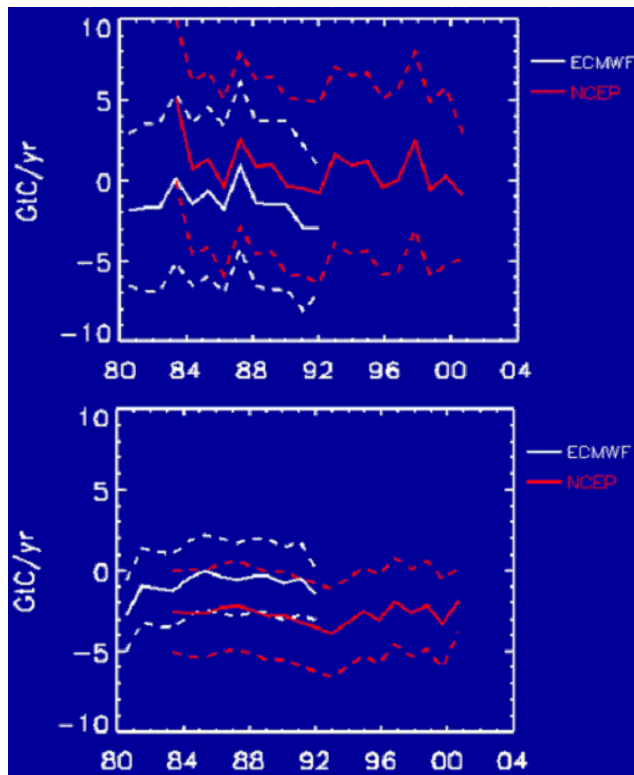
inversions but can also be aggregated in space and time for other applications (data-analysis, offline tracer transport, combined tracer inversions, low-resolution inversions, and sensitivity studies). Third, transport in TM5 was thoroughly evaluated with a new set of CMDL SF_6 observations. Knowledge of the model's transport characteristics and biases is instrumental in interpreting inversion results and properly evaluating their value.

The study with the long-lived tracer SF_6 (τ~3000 years [*Ravishankara et al.*, 1993]) indicates that the TM5 model overestimates the meridional gradient of SF_6 by ~20%, underestimates summertime SF_6 concentrations in the remote free troposphere, and overestimates SF_6 concentrations at continental locations. These discrepancies are mostly due to a lack of vertical mixing over the continents during the Northern Hemisphere summer. Temporal variability down to synoptic scales is reproduced to a very high degree, even at locations close
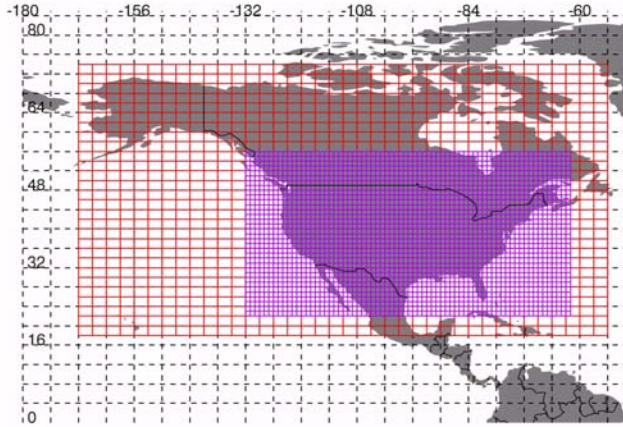
Figure 2.33. Map showing the different resolutions of TM5 for the planned CO_2 inversions. Note that the 6º × 4º grid extends over the global domain; the figure has been cropped to show more detail in the nested grid region.

to sources (Figure 2.34). This encourages the use of individual flask measurements and continuous measurements from tall towers in CO_2 inversions. Compared to a suite of similar transport models [*Denning et al.*, 1999], TM5 performs better than average and offers a number of computational advantages. Future studies of the global carbon balance with TM5 will incorporate the Kalman filter developed by CCCG to cope with the increased size of the problem as new sites are added by CMDL. Furthermore, a combination of geostatistical inverse modeling (Section 2.8.3) and high-resolution transport modeling with TM5 promises unprecedented detail in CO_2 flux-estimates for North America.
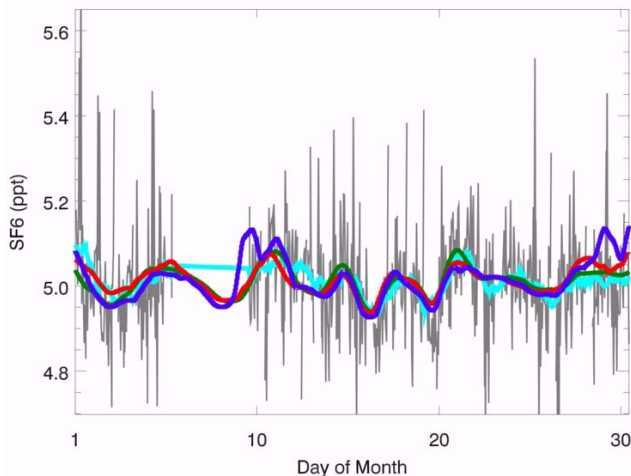

Figure 2.34. High resolution SF_6 measurements from Niwot Ridge for December 2001 (light blue), compared to the TM5 model with different nested resolutions: Global 6º × 4º (green), +North America 3º × 2º (red), ++United States 1° × 1° (purple). All curves were smoothed with a 24-hour boxcar average, original (unsmoothed) measurements shown in grey.

2.8.3. USE OF GEOSTATISTICAL INVERSE MODELING FOR CONSTRAINING BUDGETS OF ATMOSPHERIC TRACE GASES

CCGG is pioneering the application of geostatistical inverse modeling methods for estimating surface fluxes of atmospheric trace gases. Geostatistical methods have traditionally been applied to stochastic interpolation problems, defining the probability distribution of a given parameter at times or locations where it is not measured [*Cressie*, 1991; *Kitanidis*, 1997; *Matheron*, 1971]. More recently, geostatistical principles have been applied to inverse modeling problems, such as the estimation of hydraulic conductivity distributions in aquifers [*Gelhar*, 1993; *Kitanidis*, 1995; *Kitanidis and Vomvoris*, 1983; *Yeh and Zhang*, 1996; *Zimmerman et al.*, 1998] and the identification of groundwater contaminant source locations and release histories [*Michalak and Kitanidis*, 2002, 2003, 2004; *Snodgrass and Kitanidis*, 1997].

Geostatistical inverse modeling methods are a Bayesian approach in which the prior probability density function is based on an assumed model for the spatial and/or temporal covariance of the surface fluxes, and no prior flux estimates are specified. The degree to which surface fluxes at two points are expected to be correlated is defined as a function of the separation distance in space or in time between the two points. Because of its emphasis on spatial correlation, geostatistical methods are most interesting for strongly underdetermined, gridscale inversions. Flux estimates obtained using this approach are not subject to some of the limitations associated with traditional Bayesian inversions, such as potential biases created by the choice of prior flux estimates and aggregation error resulting from the use of large regions with prescribed flux patterns.

In a recent study [*Michalak et al.*, 2004] the geostatistical approach was tested using CO_2 pseudodata, generated for times when flasks were collected at 39 CMDL CCGG Cooperative Global Air Sampling Network sites, to recover surface fluxes on a 3.75° latitude by 5.0° longitude grid. Results show CO_2 surface flux variations can be recovered on a significantly smaller scale than that imposed by inversions which group surface fluxes into a small number of large regions. The estimated total surface flux distribution (comprised of fossil fuel sources, net ecosystem production, and oceanic exchange) is presented in Figure 2.35 for one of the examined cases. Small scale variations in the surface fluxes are clearly visible with large CO_2 sources in areas such as the eastern United States and western Europe.

Current work focuses on applying the method to obtain a high-resolution, multiyear estimate of the history of the surface flux variations of CO_2 using atmospheric data from the CMDL CCGG Cooperative Global Air Sampling Network. Preliminary results indicate seasonal and sub-continental scale variations can be recovered for this highly underdetermined problem without the use of prior flux estimates. The results shed light on the spatial and temporal resolution that can be identified using only the available atmospheric measurements.

Future work will involve the extension of the current applications to other trace gases (such as methane) and to regional studies (Section 2.8.2). The potential for developing an inverse model merging geostatistical prior information with prior flux estimates will also be investigated.
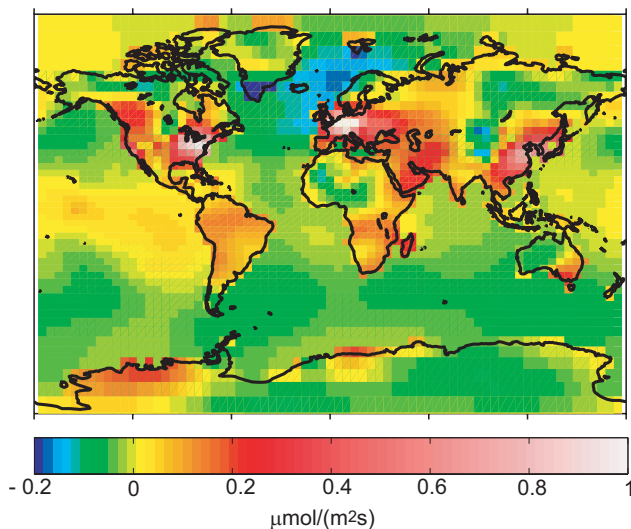
Figure 2.35. Recovered flux distribution for Case B [*Michalak et al.*, 2004]. Fluxes used for generating pseudodata were based on the work of *Andres et al.* [1996] for fossil fuels, *Takahashi et al.* [2002] for net oceanic exchange, and *McGuire et al.* [2001] for net ecosystem production. Pseudo data were sampled at actual measurement times at 39 CMDL network sites, yielding 433 samples for 2001. All three flux types were estimated using the inverse model.

2.8.4. AN APPLICATION: BAYESIAN INVERSE MODELING OF GLOBAL NITROUS OXIDE SURFACE FLUXES

The purpose of this application is to explore to what degree the CMDL CCGG Cooperative Global Air Sampling Network data can be used to constrain the budget of nitrous oxide on continental and ocean basin scales. N_2O is both a greenhouse and ozone depleting gas that enters the atmosphere through a variety of natural and anthropogenic sources. The nitrous oxide budget is currently out of balance by almost five million metric tons of nitrogen per year, resulting in an atmospheric increase of roughly one part per billion (equivalent to 0.3%) per year.

We use a Bayesian inverse modeling technique to estimate monthly average fluxes from 1997-2001 for 22 geographical regions (11 land and 11 ocean) as defined by the TransCom 3 inverse modeling study [*Gurney et al.*, 2002]. Monthly averaged measurements from 54 sites in the CCGG Cooperative Global Air Sampling Network were used to constrain the inversion, while the three-dimensional chemical transport model Tracer Model 3 (TM3) [*Heimann*, 1995] was used to specify atmospheric transport utilizing assimilated winds from NCEP. The horizontal resolution of the transport model is 5° longitude by 3.75° latitude. The regional results are aggregated to larger spatial and temporal scales, which are better constrained by the network.

Relative to the Global Emissions Inventory Activity (GEIA) global gridded flux dataset, a component of the International Global Atmospheric Chemistry Project of the International Geosphere-Biosphere Program [*Graedel et al.*, 1993; *Bouwman et al.*, 1995] that includes estimates of both natural and anthropogenic emissions for 1990, the estimated fluxes averaged over the study period suggest lower emissions from Southern

Hemisphere oceans and greater emissions from tropical land and ocean regions (Figure 2.36). Also, while the GEIA dataset does not include seasonal variations, inferred fluxes for several regions show significant seasonality, most notably in extra-tropical ocean regions where winter mixing may enhance the flux to the atmosphere [*Nevison et al.*, 1995]. Some regions, such as Northern Hemisphere land and ocean regions and the Southern Ocean, are well-constrained by the network so that the uncertainty of the surface flux estimate is reduced relative to the prior uncertainty used in the inversion. However, the regional flux estimates are generally uncertain because concentration differences between sites are not large compared to the measurement error (standard deviation of about 0.4 ppbv, based on flask pair agreement). On the global scale, we find that the CMDL flask data constrain the latitudinal distribution of the fluxes and the division between oceanic and terrestrial components of the global flux fairly well (Figure 2.36).
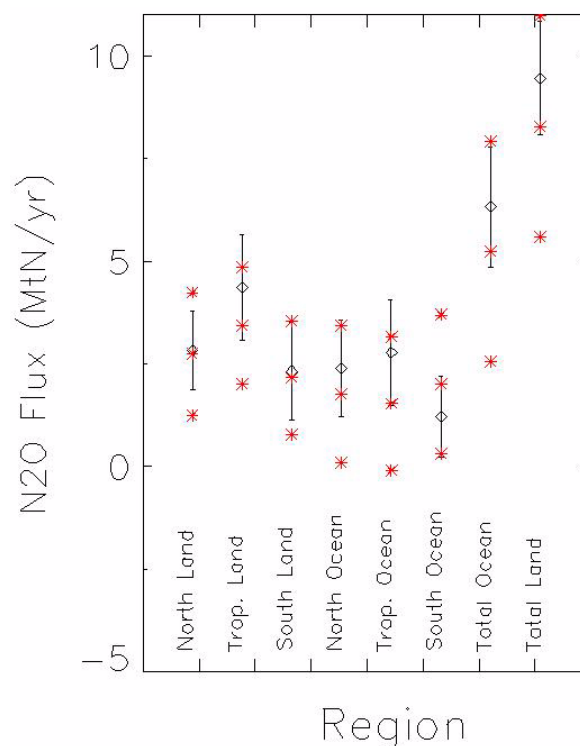

Figure 2.36. Average estimated fluxes and uncertainties for aggregated regions from 1998 to 2001. Estimated fluxes and 1σ uncertainty are shown in black for six regions: Northern Land (includes Boreal North America, Temperate North America, Europe, Northern Asia, and Central Asia), Tropical Land (Tropical South America, Northern Africa, and Southeast Asia), and Southern Land (Temperate South America, Southern Africa, and Australia/New Zealand), Northern Oceans (Arctic Ocean, Northern Pacific, and Northern Atlantic), Tropical Oceans (Western Tropical Pacific, Eastern Tropical Pacific, Tropical Atlantic, and Tropical Indian Ocean), and Southern Oceans (South Pacific, South Atlantic, South Indian, and Southern Ocean). Also shown are the 1998-2001 averages for estimated fluxes aggregated over the entire globe into Total Land and Total Ocean categories. Prior fluxes and 1σ uncertainties are shown in red for comparison. Note that the estimated fluxes are somewhat higher than the prior fluxes for the Tropical Land and Tropical Ocean regions.

2.8.5. Summary

Future modeling and data-model synthesis research activities are aimed at significant improvements in flux estimate techniques. New techniques are used to improve the numerical efficiency of inversions so that fluxes may be estimated for multiple decades with a greater number of atmospheric observations at higher spatial resolution. CCGG is investigating the use of techniques that do not rely on a priori information, and are, therefore, less subject to possible biases introduced by use of priors. Furthermore, in recognition of the fact that the surest way to improve flux estimates is to include more independent information, the plan is to use multiple species in inversions (using carbon isotope measurements in concert with CO_2 observations, for example). Also, the use of inverse techniques for estimating the budgets of other atmospheric trace species that are measured, such as N_2O, is being explored. CCGG hopes to use measurements of atmospheric tracer species with relatively well-known sources, such as SF_6, to independently estimate model representation errors (for which educated guesses are currently used). Finally, our ultimate goal is to provide routine updates of surface fluxes and their uncertainties for CO_2 and other measured atmospheric trace species as new data from the CCGG Cooperative Global Air Sampling Network become available.

2.9. References

Andres, R.J., G. Marland, I. Fung, and E. Matthews (1996), A 1 degrees ×1 degrees distribution of carbon dioxide emissions from fossil fuel consumption and cement manufacture, 1950-1990, *Global Biogeochem. Cycles*, *10*(3), 419-429.

Bakwin, P.S., P.P. Tans, B.B. Stephens, S.C. Wofsy, C. Gerbig, and A. Grainger (2003), Strategies for measurement of atmospheric column means of carbon dioxide from aircraft using discrete sampling, *J. Geophys. Res.*, *108*(D16), 4514 10.1029/2002JD003306.

Bakwin, P.S., K.J. Davis, C. Yi, S.C. Wofsy, J.W. Munger, L. Haszpra, and Z. Barcza (2004), Regional carbon dioxide fluxes from mixing ratio data, *Tellus*, in press.

Bergamaschi, P., D.C. Lowe, M.R. Manning, R. Moss, T. Bromley, and T.S. Clarkson (2001), Transects of atmospheric CO, CH_4, and their isotopic composition across the Pacific: Shipboard measurements and validation of inverse models, *J. Geophys. Res.*, *106* (D8), 7993-8011, doi:1029/2000JD900576.

Bouwman, A.F., K.W. van der Hoek, and J.G.J. Olivier (1995), Uncertainties in the global source distribution of nitrous oxide, *J. Geophys. Res.*, *100*(D2), 2785-2800, doi: 10.1029/94JD02946.

Cantrell, C.A., R.E. Shetter, A.H. McDaniel, J.G. Calvert, J.A. Davidson, D.C. Lowe, S.C. Tyler, R.J. Cicerone, and J.P. Greenberg (1990), Carbon kinetic isotope effect in the oxidation of methane by the hydroxyl radical, *J. Geophys. Res.*, *95*(D13), 22455-22462, doi:10.1029/90JD01651.

Ciais, P., P.P. Tans, J.W.C. White, M. Trolier, R.J. Francey, J.A. Berry, D.R. Randall, P.J. Sellers, J.G. Collatz, and D.S. Schimel (1995), Partitioning of ocean and land uptake of CO_2 as inferred by delta-C-13 measurements from the NOAA Climate Monitoring and Diagnostics Laboratory global air sampling network, *J. Geophys. Res.*, *100*(D3), 5051-5070, doi: 10.1029/94JD02847.

Cressie, N.A.C. (1991), *Statistics for Spatial Data*, 900 pp.,Wiley, New York.

Denning, A.S., M. Holzer, K.R. Gurney, M. Heimann, R.M. Law, P.J. Rayner, I.Y. Fung, S.M. Fan, S. Taguchi, P. Friedlingstein, Y. Balkanski, J. Taylor, M. Maiss, and I. Levin (1999), Three-dimensional transport and concentration of SF_6 - A model intercomparison study (TransCom 2), *Tellus Ser. B, 51*(2), 266-297.

Dlugokencky, E.J., L.P. Steele, P.M. Lang, and K.A. Masarie (1994a), The growth rate and distribution of atmospheric methane, *J. Geophys. Res.*, 99(D8), 17,021-17,043, doi:10.1029/94JD001245.

Dlugokencky, E.J., K.A. Masarie, P.M. Lang, P.P. Tans, L.P. Steele, and E.G. Nisbet (1994b), A dramatic decrease in the growth rate of atmospheric methane in the northern hemisphere during 1992, *Geophys. Res. Lett.*, 21(16), 45-48, doi:10.1029/94GL00606.

Dlugokencky, E.J., L.P. Steele. P.M. Lang, and K.A. Masarie (1995), Atmospheric methane at Mauna Loa and Barrow observatories: Presentation and analysis of in situ measurements, *J. Geophys. Res.*, 100(D11), 23,103-23,113, doi:10.1029/95JD02460.

Dlugokencky, E.J., E.G. Dutton, P.C. Novelli, P.P. Tans, K.A. Masarie, K.O. Lantz, and S. Madronich (1996), Changes in CH_4 and CO growth rates after the eruption of Mt. Pinatubo and their link with changes in tropical tropospheric UV flux, *Geophys. Res. Lett.*, *23*(20), 2761-2764, doi:10.1029/96GL02638.

Dlugokencky, E.J., B.P. Walter, and E.S. Kasischke (2001), Measurements of an anomalous global methane increase during 1998, *Geophys. Res. Lett.*, *28*(3), 499-503, doi:10.1029/2000GL012119.

Dlugokencky, E.J., S. Houweling, L. Bruhwiler, K.A. Masarie, P.M. Lang, J.B. Miller, and P.P. Tans (2003), Atmospheric methane levels off: Temporary pause or new steady-state?, *Geophys. Res. Lett.*, 30(19), 1992, doi:10.1029/2003GL018126.

Draxler, R.R. and G.D. Hess (1997), Description of the Hysplit_4 modeling system, *NOAA Tech. Memo ERL ARL-224*, 24 pp., National Oceanic and Atmos. Admin., Silver Spring, MD.

Duncan, B.N., I. Bey, M. Chin, L.J. Mickley, T.D. Fairlie, R.V. Martin, and H. Matsueda (2003), Indonesian wildfires of 1997: Impact on tropospheric chemistry, *J. Geophys. Res., 108*(D15), doi:10.1029/ 2002JD003195.

Emmons, L.K., M.N. Deeter, J.C. Gille, D.P. Edwards, J.L. Attié, J. Warner, D. Ziskin, G. Francis, B. Khattatov, V. Yudin, J.-F. Lamarque, S.-P. Ho, D. Mao, J.S. Chen, J. Drummond, P. Novelli, G. Sachse, M.T. Coffey, J.W. Hannigan, C. Gerbig, S. Kawakami, Y. Kondo, N. Takegawa, H. Schlager, J. Baehr, and H. Ziereis (2004), Validation of MOPITT retrievals with aircraft in situ profiles, *J. Geophys. Res.*, *109*, D03309, doi:10292003JD004101.

Gelb, A. (1974), *Applied Optimal Estimation*, 374 pp., MIT Press, Cambridge, MA.

Gelhar, L.W. (1993), *Stochastic Subsurface Hydrology*, 390 pp., Simon & Schuster, New York.

Gemery, P.A., M. Trolier, and J.W.C. White (1996), Oxygen isotope exchange between carbon dioxide and water following atmospheric sampling using glass flasks, *J. Geophys. Res.*, *101*(D9), 14,415-14,420, doi:10.1029/96JD00053.

Gerbig, C., D. Kley, A. Voltz-Thomas, J. Kent, K. Dewey and D.S. McKenna (1996), Fast-response resonance fluorescence CO measurements aboard the C-130: Instrument characterization and measurements made during North American Regional Experiment 1993, *J. Geophys. Res., 101*(D22), 29,229-29,238, doi:10.1029/ 95JD03272.

Gerbig, C., J.C. Lin, S.C. Wofsy, B.C. Daube, A.E. Andrews, B.B. Stephens, P.S. Bakwin, and A. Grainger (2003a), Towards constraining regional scale fluxes of CO_2 with atmospheric observations over a continent: 1. Observed spatial variability from airborne platforms, *J. Geophys. Res.*, *108*(D24), 4756, doi:10.1029/2002JD003018.

Gerbig, C., J.C. Lin, S.C. Wofsy, B.C. Daube, A.E. Andrews, B.B. Stephens, P.S. Bakwin, and A. Grainger (2003b), Towards constraining regional scale fluxes of CO_2 with atmospheric observations over a continent: 2. Analysis of COBRA data using a receptor oriented framework, *J. Geophys. Res.*, *108*(D24), 4757, doi:10.1029/2002JD003770.

GLOBALVIEW-CH_4 (2001), Cooperative Atmospheric Data Integration Project-Methane [CD-ROM], NOAA Clim. Monit. and Diagnostics Lab., Boulder, CO (also available on Internet via anonymous FTP to ftp.cmdl.noaa.gov, Path: ccg/ch4/GLOBALVIEW).

GLOBALVIEW-CO_2 (2003), Cooperative Atmospheric Data Integration Project-Carbon Dioxide [CD-ROM], NOAA Clim. Monit. and Diagnostics Lab., Boulder, CO (also available on Internet via anonymous FTP to ftp.cmdl.noaa.gov, ccg/co2/GLOBALVIEW).

Gloor, M., P. Bakwin, P. Tans, D. Hurst, L. Lock, and R. Draxler, (2001), What is the concentration footprint of a tall tower? *J. Geophys. Res.* *106*(D16), 17,831-17,840, doi:10.1029/JD900021.

Graedel, T.E., T.S. Bates, A.F. Bouwman, D. Cunnold, J. Dignon, I. Fung, D.J. Jacob, B.K. Lamb, J.A. Logan, G. Marland, P. Middleton, J.M. Pacyna, M. Placet, and C. Veldt (1993), A compilation of inventories of emissions to the atmosphere, *Global Biogeochem. Cycles*, *7*(1), 1-26.

Gurney, K.R., R.M. Law, A.S. Denning, P.J. Rayner, D. Baker, P. Bousquet, L. Bruhwiler, Y.H. Chen, P. Ciais, S. Fan, I.Y. Fung, M. Gloor, M. Heimann, K. Higuchi, J. John, T. Maki, S. Maksyutov, K. Masarie, P. Peylin, M. Prather, B.C. Pak, J. Randerson, J. Sarmiento, S. Taguchi, T. Takahashi, and C.W. Yuen (2002), Towards robust regional estimates of CO_2 sources and sinks using atmospheric transport models, *Nature*, *415*(6872), 626-630.

Heimann, M. (1995), The global atmospheric tracer model TM2, *Tech. Rep. No. 10*, 53 pp., Klimarechenzentrum, Max Planck Institut fur Meteorol., Germany.

Hein, R., P.J. Crutzen, and M. Heimann (1997), An inverse modeling approach to investigate the global atmospheric methane cycle, *Global Biogeochem. Cycles*, *11*(1), 43-76.

Houweling, S., F. Dentener, J. Lelieveld, B. Walter, and E. Dlugokencky (2000), The modeling of tropospheric methane: How well can point measurements be reproduced by a global model?, *J. Geophys. Res.*, *105*(D7), 8981-9002, doi:10.1029/1999JD901149.

Hurst, D.F., P.S. Bakwin, R.C. Myers, and J.W. Elkins (1997), Behavior of trace gas mixing ratios on a very tall tower in North Carolina, *J. Geophys. Res.*, *102*(D7), 8825-8835, doi:10.1029/97JD00130.

Hurst, D.F., P.S. Bakwin, and J.W. Elkins (1998), Recent trends in the variability of halogenated trace gases over the United States, *J. Geophys. Res.*, *103*(D19), 25,299-25,306, doi:10.1029/98JD01879.

Kalman, R.E. (1960), A new approach to linear filtering and prediction problems, *J. Basic Eng. (ASME)*, *82D*, 35-45.

King, D.B., R.C. Schnell, R.M. Rosson, and C. Sweet (Eds.) (2002), *Climate Monitoring and Diagnostics Laboratory Summary Report No. 26 2000-2001*, pp. 28-50, National Oceanic and Atmos. Admin., Boulder, CO.

Kitanidis, P.K. (1995), Quasi-Linear Geostatistical Theory for Inversing, *Water Resour. Res.*, *31*(10), 2411-2419.

Kitanidis, P.K. (1997), *Introduction to Geostatistics: Applications in Hydrogeology*, 271 pp., Cambridge University Press, New York.

Kitanidis, P.K., and E.G. Vomvoris (1983), A Geostatistical Approach to the Inverse Problem in Groundwater Modeling (Steady-State) and One-Dimensional Simulations, *Water Resour. Res.*, *19*(3), 677-690.

Kitzis, D. and C. Zhao (1999), CMDL/Carbon Cycle Gases Group Standards Preparation and Stability. *NOAA Tech. Memo. ERL CMDL-14*, 14 pp., National Oceanic and Atmos. Admin., Boulder, CO.

Langenfelds, R.L., R.J. Francey, B.C. Pak, L.P. Steele, J. Lloyd, C.M. Trudinger, and C.E. Allison (2002), Interannual growth rate variations of atmospheric CO_2, $\delta^{13}C$, H_2, CH_4, and CO between 1992 and 1999 linked to biomass burning, *Global Biogeochem. Cycles*, *16*(3), 1048. doi:10.1029/2001GB001466.

Levine, J. (1999), The 1997 fires in Kalimantan and Sumatra, Indonesia: Gaseous and particulate emissions, *Geophys. Res. Lett., 26*(7), 815-818, doi:10.1029/1999GL900067.

Lloyd, J., and G.D. Farquhar (1994), C-13 discrimination during CO_2 assimilation by the terrestrial biosphere, *Oecologia*, *99* (3-4), 201-215.

Marland, G., T.A. Boden, and R.J. Andres (2002), Global, regional and national fossil fuel CO_2 emissions, in *Trends: A Compendium of Data on Global Change,* (http://cdiac.esd or nl.gov/trends.htm) Carbon Dioxide Information Analysis Center, Oak Ridge Nat. Lab., U.S. Dept. of Energy, Oak Ridge, TN.

Masarie, K.A., L.P. Steele, and P.M. Lang (1991), A rule-based expert system for evaluating the quality of long-term, in situ gas chromatographic measurements of atmospheric methane, *NOAA Tech. Memo. ERL CMDL-3*, National Oceanic and Atmos. Admin., Boulder, CO.

Masarie, K.A., and P.P. Tans (1995), Extension and integration of atmospheric CO_2 data into a globally consistent measurement record, *Procceedings of* the *8th WMO Meeting of Experts on Carbon Dioxide Concentration and Isotopic Measurement Techniques*, Boulder, CO, 6-11 July 1995, edited by T. Conway, pp. 11-19.

Masarie, K.A., R.L. Langenfelds, C.E. Allison, T.J. Conway, E.J. Dlugokencky, R.J. Francey, P.C. Novelli, L.P. Steele, P.P. Tans, B. Vaughn, and J.W.C. White (2001), The NOAA/CSIRO flask-air intercomparison program: A strategy for directly assessing consistency among atmospheric measurements derived from independent laboratories, *J. Geophys. Res.*, *106*(D17), 20,445-20,464, doi:10.1029/2000JD000023.

Masarie, K.A., and P.P. Tans (2003), Updated guidelines for atmospheric trace gas data management, *WMO GAW TD 1149,* 41 pp., World Meteorol. Organ., Geneva.

Matheron, G. (1971), *The Theory of Regionalized Variables and Its Applications*, 211 pp., École National Supérieure des Mines, France.

McGuire, A.D., S. Sitch, J.S. Clein, R. Dargaville, G. Esser, J. Foley, M. Heimann, F. Joos, J. Kaplan, D.W. Kicklighter, R.A. Meier, J.M. Melillo, B. Moore, I.C. Prentice, N. Ramankutty, T. Reichenau, A. Schloss, H. Tian, L.J. Williams, and U. Wittenberg (2001), Carbon balance of the terrestrial biosphere in the twentieth century: Analyses of CO_2, climate and land use effects with four process-based ecosystem models, *Global Biogeochem. Cycles*, *15*(1), 183-206.

Michalak, A.M., and P.K. Kitanidis (2002), Application of Bayesian inference methods to inverse modeling for contaminant source identification at Gloucester Landfill, Canada, in *Computational Methods in Water Resources XIV,* edited by S.M.Hassanizadeh, R.J. Schotting, W.G. Gray, and R.J. Schotting., pp. 1259-1266, Elsevier, Amsterdam.

Michalak, A.M., and P.K. Kitanidis (2003), A method for enforcing parameter nonnegativity in Bayesian inverse problems with an application to contaminant source identification, *Water Resour. Res.*, *39*(2) 1033-1046, doi:10.1029/2002WR001480.

Michalak, A.M., and P.K. Kitanidis (2004), Application of geostatistical inverse modeling to contaminant source identification at Dover AFB, Delaware, *J. Hydraul. Res.*, *42* (extra issue) pp. 9-18.

Michalak, A.M., L.M. Bruhwiler, and P.P. Tans (2004), A geostatistical approach to surface flux estimation of atmospheric trace gases, *J. Geophys. Res.*, in press.

Miller, J.B., K.A. Mack, R. Dissly, J.W.C. White, E.J. Dlugokencky, and P.P. Tans (2002), Development of analytical methods and measurements of $^{13}C/^{12}C$ in atmospheric CH_4 from the NOAA/CMDL global air sampling network, *J. Geophys. Res.*, *107*(D13), doi: 10.1029/2001JD000630.

Montzka, S.A., C.M. Spivakovsky, J.H. Butler, J.W. Elkins, L.T. Lock, and D.J. Mondeel (2000), New observational constraints for atmospheric hydroxyl on global and hemispheric scales, *Science*, *288*(5345), 500-503.

Nevison, C.D., R.F. Weiss, and D.J. Erickson (1995), Global oceanic emissions of nitrous-oxide, *J. Geophys. Res.*, *100*(C8), 15,809-15,820, doi:10.1029/95JC00684.

Novelli, P.C., J.W. Elkins, and L.P. Steele (1991), The development and evaluation of a gravimetric reference scale for measurements of atmospheric carbon monoxide, *J. Geophys. Res.*, *96*(D7), 13,109-13,121, doi:10.1029/91JD01108.

Novelli, P.C., K.A. Masarie, P.M. Lang, B.D. Hall, R.C. Myers, and J.W. Elkins (2003), Reanalysis of tropospheric CO trends: Effects of the 1997-1998 wildfires, *J. Geophys. Res.*, *108*(D15), 4464, doi:10.1029/2002JD003031.

Olivier, J.G.J. and J.J.M. Berdowski (2001), Global emission sources and sinks, in *The Climate System*, edited by J. Berdowski, R. Guichert, and B. Heij, pp. 33-37, Swets and Zeitlinger, The Netherlands.

Olivier, J.G.J. (2002), On the quality of global emission inventories, approaches, methodologies, input data and uncertainties, PhD Thesis, section 4.2, pp. 58-90, Utrecht University, The Netherlands.

Pacala S.W., G.C. Hurtt, R.A. Houghton, R.A. Birdsey, L. Heath, E.T. Sundquist, R.F. Stallard, D. Baker, P. Peylin, P. Ciais, P. Moorcraft, J. Caspersen, E. Shevliakova, B. Moore, G. Kohlmaier, E. Holland, M. Gloor, M.E. Harmon, S.-M. Fan, J.L. Sarmiento, C. Goodale, D. Schimel, and C.B. Field (2001), Consistent land- and atmosphere-based U.S. carbon sink estimates, *Science*, *292*(5525), 2316-2320.

Quay, P., J. Stutsman, D. Wilbur, A. Snover, E. Dlugokencky, and T. Brown (1999), The isotopic composition of atmospheric methane, *Global Biogeochem. Cycles*, *13*(2), 445-461.

Ravishankara, A.R., S. Solomon, A.A. Turnipseed, and R.F. Warren (1993), Atmospheric lifetimes of long-lived halogenated species, *Science*, *259* (5092), 194-199.

Snodgrass, M.F., and P.K. Kitanidis (1997), A geostatistical approach to contaminant source identification, *Water Resourc. Res.*, *33*(4), 537-546.

Takahashi, T., S.C. Sutherland, C. Sweeney, A. Poisson, N. Metzl, B. Tilbrook, N. Bates, R. Wanninkhof, R.A. Feely, C. Sabine, J. Olafsson, and Y. Nojiri (2002), Global sea-air CO_2 flux based on climatological surface ocean pCO(2), and seasonal biological and temperature effects, *Deep-Sea Res. II*, *49*(9-10), 1601-1622.

Tans, P.P., J.A. Berry, and R.F. Keeling (1993), Oceanic $^{13}C/^{12}C$ observations: A new window on ocean CO_2 uptake, *Global Biogeochem. Cycles*, *7*(2), 353-368.

Tans, P.P. et al. (2002), Carbon Cycle, in *Climate Monitoring and Diagnostics Laboratory Summary Report No. 26, 2000-2001*, edited by D.B. King, R.C. Schnell, R.M. Rosson, and C. Sweet, pp. 28-50, National Oceanic and Atmos. Admin., Boulder, CO.

Thoning, K.W., P.P. Tans, and W.D. Komhyr (1989), Atmospheric carbon dioxide at Mauna Loa, 2, Analysis of the NOAA GMCC data 1974-1985, *J. Geophys. Res.*, *94*(6), 8549-8576, doi:10.1029/89JD00315.

van der Werf, G.R., J.T. Randerson, G.J. Collatz, L. Giglio, P.S. Kasibhatla, A.F. Arellano, Jr., S.C. Olsen, and E.S. Kasischke (2004), Continental-scale partitioning of fire emissions during the 1997 to 2001 El Niño/La Niña period, *Science*, *303*(5654), 73-76.

Walter, B.P. (1998), Development of a process-based model to derive methane emissions from natural wetlands for climate studies, PhD Thesis, Max-Planck-Instit. Für Meteorol., Hamburg, Germany.

Walter, B.P., and M. Heimann (2000), A process-based, climate sensitive model to derive methane emissions from natural wetlands: Applications to five wetland sites, sensitivity to model parameters and climate, *Global Biogeochem. Cycles*, *14*(3), 745-766, doi:10.1029/1999GB001204.

WMO (World Meteorological Organization) (1981), Scientific requirements, in *Report of the WMO/UNEP/ICSU Meeting on Instruments, Standardization and measurement techniques for atmospheric CO$_2$*, Geneva, Switzerland, 8-11 September.

Wofsy, S.C., and R.C. Harriss (2002), *The North American Carbon Program (NACP)*, U.S. Global Change Research Program, NACP Comm. of the U.S. Interagency Carbon Cycle Science Program, Washington, D.C., 56 pp.

Wotawa, G., P.C. Novelli, M. Trainer, and C. Granier (2001), Interannual variability of summertime CO concentrations in the Northern Hemisphere explained by boreal forest fire in North America and Russia, *Geophys. Res. Lett.*, *28*(24), 4575-4578, doi:10.1029/2001GL013686.

Yeh, T.-C.J., and J. Zhang (1996), A geostatistical inverse method for variably saturated flow in the vadose zone, *Water Resour. Res.*, *32*(9), 2757-2766.

Zhang, J., P.D. Quay, and D.O. Wilbur (1995), Carbon isotope fractionation during gas-water exchange and dissolution of CO_2, *Geochim. Cosmochim. Acta*, *59*(1), 107.

Zhao, C., P. Tans, and K. Thoning, (1997): A manometric system for absolute calibrations of CO_2 in dry air. *J.Geophys. Res.*, *102*(D5), 5885-5894, doi:10.1029/96JD03764.

Zimmerman, D.A., G. de Marsily, C.A. Gotway, M.G. Marietta, C.L. Axness, R.L. Beauheim, R.L. Bras, J. Carrera, G. Dagan, P.B. Davies, D.P. Gallegos, A. Galli, J. Gomez-Hernandez, P. Grindrod, A.L. Gutjahr, P.K. Kitanidis, A.M. Lavenue, D. McLaughlin, S.P. Neuman, B.S. RamaRao, C. Ravenne, and Y. Rubin (1998), A comparison of seven geostatistically based inverse approaches to estimate transmissivities for modeling advective transport by groundwater flow, *Water Resour. Res.*, *34*(6), 1373-1413.